T.C.
INONU UNIVERSITY
GRADUATE SCHOOL OF NATURAL AND APPLIED SCIENCES

URICASE IMMOBILIZATION ON NANOFIBER MEMBRANES PREPARED BY ELECTROSPINNING AND ITS USE AS VOLTAMMETRIC URIC ACID BIOSENSOR

MASTER THESIS

Fakhriy MUHAMMAD

DEPARTMENT OF CHEMISTRY

MALATYA
MAY 2022

T.C.
INONU UNIVERSITY
GRADUATE SCHOOL OF NATURAL AND APPLIED SCIENCES

URICASE IMMOBILIZATION ON NANOFIBER MEMBRANES PREPARED BY ELECTROSPINNING AND ITS USE AS VOLTAMMETRIC URIC ACID BIOSENSOR

MASTER THESIS

Fakhriy MUHAMMAD

36183613014

DEPARTMENT OF CHEMISTRY

Supervisor : Prof. Dr. Burhan Ates
Co – Supervisor : Assoc. Prof. Dr. Ahmet Ulu

MALATYA
MAY 2022

ACKNOWLEDGEMENTS

I would like to acknowledge and give my warmest gratitude for the supervision and guidance to my first supervisor Prof. Dr. Burhan Ateş and Assoc. Prof. Dr. Ahmet Ulu. Thus, in this pandemic, I am able to accomplish my thesis research. Also my family member : my father Amir Faisal, my mother Dina Sakinah and my sister Araniy Fadhilah for the continuous support in my thesis research and life.

Also, I am highly grateful Thanks to our lab colleagues for the cooperation and assistance in this thesis research, to Gamze Dik for enzyme activity work, to Seda Kolak and Kübra Karadaş for the polymer work and electrospinning. Also, to other lab friend for method discussion Dr. Samer Abbas Ali Noma. Also, to İmren Özcan for FTIR test at Physical Chemistry Laboratory.

In addition, special thanks to my Lecturers in my almamater, Bogor Agricultural University (IPB), Bogor, Indonesia to Prof. Dr. Dyah Iswantini and Dr. Mohammad Khotib for the consultation of electrochemical method and polymer coating system and to Dr. Laksmi Ambarsari for enzyme immobilization method. Also, for my friend in IPB Dr. Ali Aulia Ghozali for the discussion of electrochemical parameters.

This study was supported by İnönü University, Scientific Research Projects (İNÖNÜ-BAP) Unit (Project number: FYL-2021-2567). I would like to thank İnönü University, which provided financial support.

DECLARATION

I would like to declare that my master thesis which entitled “Uricase Immobilization on Nanofibre Membranes Prepared by Electrospinning and its Use as Voltammetric Uric Acid Biosensor”, the content of my thesis is my own work. This thesis has not been submitted for any degree or other purposes.

I also certify that the intellectual content of this thesis is product of my own mind and work as well as acknowledged source of assistance.

Fakhriy MUHAMMAD

TABLE OF CONTENTS

LIST OF TABLES

LIST OF FIGURES

ABBREVIATIONS

AA : Ascorbic Acid

CE : Counter Electrode

CV : Cyclic Voltammetry

DMF : Dimethyl Formamide

DPV : Differential Pulse Voltammetry

EA : Electroactive Area

EDX : Energy Dispersive X – Ray

EIS : Electrochemical Impedance Spectroscopy

FTIR : Fourier Transform Infra Red

GA : Glutaraldehyde

I peak : Peak Current

Ipa : Anode Peak Current

Ipc : Cathode Peak Current

MB : Methylene Blue

Non MB : Non Methylene Blue

PBS : Phosphate Buffer Saline

PEI : Polyethylene Imine

PCL : Polycaprolactone

RE : Reference Electrode

SEM : Scanning Electron Microscope

QD SPCE : Quantum Dot Screen Printed Electrode

UA : Uric Acid

UOx : Uric acid oxidase or uricase

WE : Working Electrode

XRD : X – Ray Diffraction

ÖZET

Y. Lisans Tezi

Elektroeğirme ile Hazırlanan Nanofiber Membranlara Ürikaz İmmobilizasyonu ve voltammetrik Ürik Asit Biyosensörü Olarak Kullanımı

Fakhriy MUHAMMAD

İnönü Üniversitesi
Fen Bilimleri Enstitüsü
Kimya Bölümü

64 + x sayfa

2022

Ürik asit klinikte gut ve hiperürisemi başta olmak üzere çeşitli hastalıkların belirteci olarak kullanılmaktadır. Bu nedenle serum ve gıda örnekleri gibi biyolojik numuneler hassas bir şekilde ölçümü oldukça önemlidir. Ürikaz (ürat oksidaz, E.C.1.7.3.3, UOx) vücutta ürik asidin allantoine oksidasyonundan sorumlu enzim olup özellikle *in vitro* ürik asit düzeyeni ölçmede yaygın kullanımı mevcuttur. Uygulamada ürik asit tayinine yönelik kolorimetrik, kromotografik, spektrofotometrik ve biyosensör temelli yöntemler mevcuttur. Bununla beraber özellikle hızlı sonuç veren, seçici ve kolay kullanılabilir sistemlerin oluşturulması ürik asit tayini için hala önemli bir ihtiyaçtır. Bu çalışmada ürik asidin seçici ve hassas bir şekilde belirlenmesi için elektroeğirme ile hazırlanan membranlar içeren perde baskılı elektrotların hazırlanması, ürikaz enziminin immobilizasyonu ve amperometrik ürik asit biyosensörü olarak kullanılması mevcuttur.

Bu kapsamda elektroeğirme hazırlanan membranda mekanik mukavemeti nedeniyle polikaprolakton (PCL, % 10) ve enzimin immobilizasyonu için amin grubu içeren polietilenimin'den (PEI, % 7.5) faydalanılmıştır. İki farklı membran içeren Quantum Dot Screen Printed Electrode (QD - SPCE) hazırlanmıştır. Bunlardan biri PCL/PEI /UOx /QD – SPCE, diğeri ise metilen mavisi (MB) ile desteklenmiş PCL/PEI/UOx/MB/QD–SPCE şeklindedir. Hazırlanan membranlar yapısal olarak FTIR, EDX ve XRD, morfolojik açıdan SEM ve hidrofiliklik açıdan sıvı temas açısı ile karakterize edilmiştir. Voltametrik ölçümlerde standardizasyon, PBS pH 7.4'te 5 ve 52 μM arasında ürik asit (UA) konsantrasyonu için DPV (Diferansiyel Puls Voltametrisi) tekniği ile gerçekleştirilmiştir. Sonuçlar UOx/QD–SPCE için LOD:3,9619 ± 0,588 μM (R^2 = 0.9947) iken UOx/MB/QD–SPCE için LOD:1,8598 ± 0,2345 μM (R^2 = 0.9988) olarak tespit edilmiştir. 4 haftalık stabilite sonuçları UOx/QD–SPCE ve UOx/MB/QD–SPCE için akımdaki değişimi sırasıyla %92 ve %87 olduğunu göstermiştir. Ayrıca interferansları içeren karışım çözeltisi kullanıldığında ürik asit için akım oranları UOx/QD–SPCE ve UOx/MB/QD–SPCE elektrolar için sırasıyla %95 ve %82 gerçekleşmiştir.

Sonuç olarak hazırlanmış iki biyosensör sisteminde ürik asit ölçümünde literatürdeki sensörler ile karşılaştırılabilir düzeyde ölçüm niteliklerine sahip olduğu tespit edilmiştir.

Anahtar Kelimeler: Urikaz, biyosensor, elektroeğirme, nanofiber membran, polikaprolakton

ABSTRACT

Master Thesis

Uricase Immobilization on Nanofibre Membranes Prepared by Electrospinning and its Use as Voltammetric Uric Acid Biosensor

Fakhriy MUHAMMAD

Inonu University
Graduate School of Natural and Applied Sciences
Chemistry Department

64 + x pages

2022

Uric acid (UA) is clinically used as a marker of various diseases, especially gout and hyperuricemia. Therefore, precise measurement of biological samples such as serum and food samples is crucial. Uricase (urate oxidase, E.C.1.7.3.3, UOx) is the enzyme responsible for the oxidation of UA to allantoin in the body, and it is widely used especially in measuring UA level *in vitro*. In practice, there are colorimetric, chromatographic, spectrophotometric and biosensor-based methods for UA determination. However, a crucial need for determination of UA is exist, especially the creation of rapid results, selective and easy-to-use systems. In this study, the preparation of screen-printed electrodes containing membranes prepared by electrospinning, immobilization of UOx enzyme and its use as an voltammetric UA biosensor for the selective and sensitive determination of UA are available.

In this context, polycaprolactone (PCL, 10%) was used in the membrane prepared by electrospinning due to its mechanical strength, and polyethyleneimine containing amine group (PEI, 7.5%) was used for the immobilization of the enzyme. Quantum Dot Screen Printed Electrode (QD - SPCE) containing two different membranes was prepared. One of them is PCL/PEI /UOx /QD – SPCE, the other is PCL/PEI/UOx/MB/QD–SPCE supplemented with methylene blue (MB). The prepared membranes were structurally characterized by FTIR, EDX and XRD, morphologically by SEM and voltammetric by water contact angle. Standardization in was performed by DPV (Differential Pulse Voltammetry) technique for UA concentration between 5 and 52 μM in PBS pH 7.4. Results were determined as LOD: 3.9619 ± 0.588 μM (R^2 = 0.9947) for UOx/QD–SPCE, while LOD: 1.8598 ± 0.2345 μM (R^2 = 0.9988) for UOx/MB/QD–SPCE. The 4-week stability results showed the change in current for UOx/QD–SPCE and UOx/MB/QD–SPCE to be 92% and 87%, respectively. In addition, in the mixed interference test remaining current ratios for UA were 95% and 82% for the UOx/QD–SPCE and UOx/MB/QD–SPCE electrodes, respectively.

As a result, it has been determined that the two prepared biosensor systems have comparable measurement qualities with the sensors in the literature in UA measurement.

Key Words : Uricase, biosensor, electrospinning, nanofiber membrane, polycaprolactone,

1. INTRODUCTION

Certain specific target analyte from biological samples is detectable by biosensor with immobilized biological recognition element for example enzyme, nucleic acid, cell and antibody. Subsequently specific interaction between target analyte and transducer will generate physicochemical signal such as piezoelectric, optical and electrochemical. Enzymatic biosensor is constructed by three components: biological recognition element, transducer and signal processing system. In particular, enzymatic electrochemical biosensor utilizes immobilized enzyme as recognition element which carries out redox reaction. Consequently, electrochemical signal is released in transducer surface as output for example: current, voltage, resistance and superficial change. Owing to the mechanism, biosensor particularly electrochemical based possesses a number of advantages: simplicity, rapidity, low cost and sensitivity (Nguyen *et al*. 2019).

As a result of purine breakdown in metabolism, uric acid (UA) is generated and subsequently flows in blood and urine with normal range from 0.14 to 0.4 mmol dm^{-3} and 1.5 to 4.5 mmol dm^{-3} respectively. A number of factors lead the alteration of UA concentration with clinical consequences particularly age and gender. Hyperuricemia, the elevation of UA in blood serum leads a number of diseases such as gout, cardiovascular disease, Lesch–Nyhan syndrome and type 2 diabetes. In contrast, decreasing UA level lead neurodegenerative diseases such as Parkinson and Alzheimer diseases (Mazzara *et al*. 2021).

A number of existing UA measurement methods are invasive as it requires blood sampling. Moreover, conventional methods are time consuming, complex and is not suit the personal use. For example: High-performance liquid chromatography (HPLC), gas chromatography (GC), spectrophotometry and fluorimetry. Particularly, HPLC and spectrophotometric methods require sample pretreatment and harmful solvent. Hence electrochemical techniques has become a current trend in recent decades due to its rapidity and reliability. Nevertheless, the weak point of electrochemical method is low selectivity to analyze the target molecule. Moreover, uricase (UOx) enzyme has been utilized to modify the electrode for improving its selectivity (Fukuda *et al*. 2020).

Apart from enzymatic modification, polymer modification of electrode has been applied as both of enzyme immobilization agent and selectivity agent particularly redox

polymer. Moreover, mediator is also mixed in polymer composite as electron transfer agent. Consequently, efficient wiring of enzyme is achieved as a result of polymer deposition. Furthermore, electrospinning application for electrode coating has taken recent attention as it improves selectivity by the formation of nanopores between fibers (Szczesny *et al*. 2020). Also, Quantum dot (QD) particularly cadmium selenium (CdSe) has been utilized to modify electrode due to its semiconductor properties. Subsequently, interaction between redox species and QD has been relied efficiently as electrochemical signal (Ridel *et al*. 2017 and Martin – Yerga *et al*. 2017).

In this following thesis, we aim to construct and research an electrochemical based enzymatic biosensor with UOx enzyme immobilization in PCL – PEI nanofiber and coat the QD SPCE to measure UA by voltammetric method.

2. THEORETICAL INVESTIGATION

2.1. Electrochemical Biosensor

Biosensor, a major breakthrough in analytical chemistry has been emerged since 1960s and continuously developing until today. Owing to IUPAC definition, an analytical system is considered as biosensor as long as it incorporates biological sensing system. In addition, pre – separation steps and sample processing are not required in assay. Biosensors is classified in accordance to biological components and transducers. For biological components it is classified as macromolecules (enzyme, DNA and antibody), cell fragments (membrane and organelle) and whole cells (tissue and microorganisms). Meanwhile for transducers classification it consists of : electrochemical, optical and others (piezoelectric and calorimetric) (Monteiro and Almeida 2019).

Electrochemical biosensor consists of three electrode system : Working (WE), Counter (CE) and Reference (RE) Electrode, in which analog principles from electroanalytical cells is developed. Moreover, the electron transfer has been widely utilized as a ground of electrochemical analysis that involves both of electron transfer into the surface of WE as well as continuing current flow into the counter electrode. Apart from this, a number of enzyme immobilization has been required and carried out to improve its selectivity and reliability. In accordance to the principle of electrode system, enzyme is immobilized in working electrode with certain agents (Weltin *et al*. 2016 and Taurino *et al*. 2016).

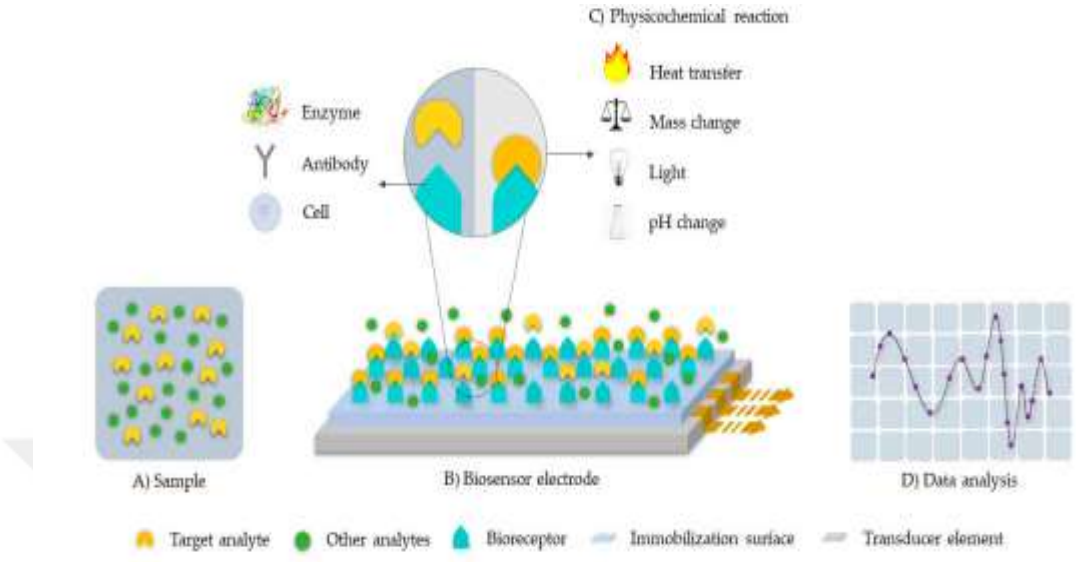

Figure 1 : General work scheme of electrochemical biosensor with distinguished types of molecular recognizing agents (enzyme, antibody or cell) (Campana *et al*. 2019)

2.1.1. Generations of electrochemical biosensor

Electrochemical biosensor is divided into three generations which is also consist of 2.5 generation. For starter, first generation biosensor relies on electron shuttle and H_2O_2 as electrochemical signal from enzymatic reaction. Thereafter, second generation biosensor relies on oxidation and reduction of mediator for electron transport from enzymatic hydrolyzed species. Then, 2.5 generation carries out analysis by quasi – direct electron transfer as it uses both of mediators and conductive polymer surface. Meanwhile third generation relies on direct electron transfer between catalyzed analyte and electrode surface (Suzuki *et al*. 2020).

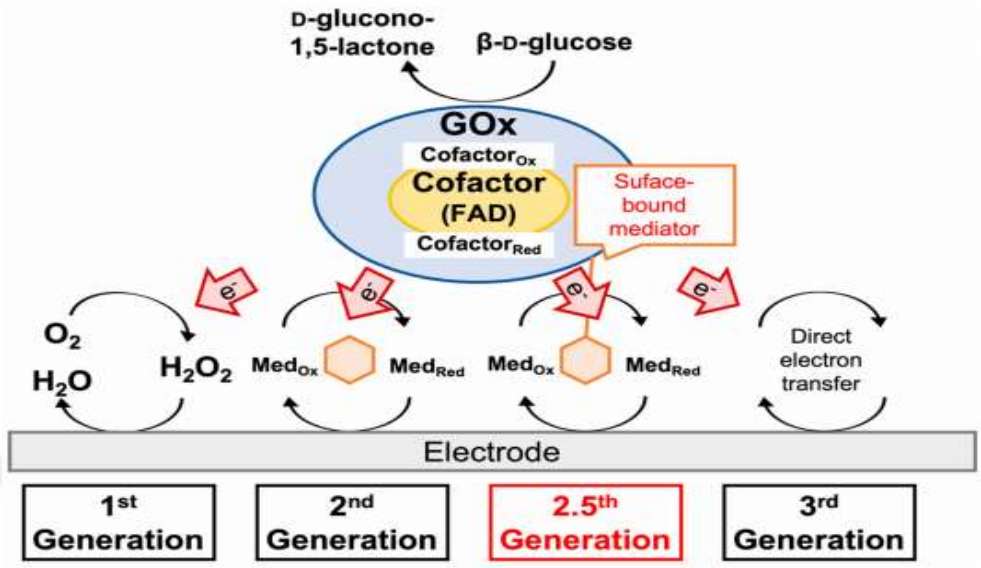

Figure 2 : Schematic work principle of Glucose oxidase enzymatic biosensor in various generation (Suzuki *et al*. 2020)

Third generation biosensor has created distinct engineering feature to enable direct electron transfer into the electrode surface. Consequently, protein engineering methods is implemented to place the active site oppositely electrode surface. Moreover, surface engineering is required for example interfacial technologies and carbon based nanomaterials. Moreover, dehydrogenase enzyme has been implemented in 3rd generation biosensor due to the release of FAD or PQQ. Subsequently, direct electron transfer is facilitated (Bollela *et al*. 2018).

One clear example, nitric oxide reductase was utilized to construct 3rd generation biosensor for nitric oxide detection by immobilization in multiwall carbon nanotube (MWCNT) / 1 – n – butyl – 3 – methylimidazolium tetrafluoroborate ($BMIMBF_4$). Consequently, MWCNT and $BMIMBF_4$ roled both as enzyme immobilization agent and electron transfer due to its inert properties (Gomes *et al*. 2019). In addition, Musameh *et al*. (2018) researched the heme silk - MWCNT as modification agent of glassy carbon electrode (GCE) for the detection of nitric oxide. Owing to folding properties of heme protein, manipulations will drive the regulation which affect the binding and electron release. Hence, 3rd generation biosensor is generated.

2.2.Enzymatic Biosensor

In the enzymatic biosensor, it was noted that enzymatic conversion of target substrate (analyte) releases the electrochemical signal (Asal *et al*. (2018) and Campana *et al*. (2019)). Furthermore, this electrochemical signal is forwarded into the transducers; for example : electrochemical, optical an calorimetric transducer. Moreover, the signal is displayed digitally by specialized software of computer. Apart from this, incorporation of enzyme immobilizing materials is required to incorporate the enzyme and electrode; for example: carbon nanotubes, nanoparticles, polymers and chitosan for glucose oxidase enzyme immobilization into the screen printing electrode. One clear example, immobilization of horseradish peroxidase, choline kinase and choline oxidase on the acrylic microspheres leads the cascade reaction by releasing the detectible H_2O_2 as electrochemical signal.

Alteration within the narrow potential window from - 1 to + 1 Volt by the regulated reduction oxidation reaction by oxidoreductase enzyme. Hence, electron transfer takes place as electrochemical signal which represent the concentration of certain biomolecules analytes. Lee *et al*. (2018) also noted that the surface functionalization within the instrumental design also takes a role in both of the enzyme immobilization as well as cavity formation to adsorb the target analytes. Apart from this, various number of biological molecules that is found in tears, saliva, intestinal fluid and sweat possess its own normal range. Hence, enzymatic biosensor is able to calculate the analytes in body fluid outside blood as non invasive method (Monteiro and Almeida 2019).

Apart from this, in the review of Rocchita *et al*. (2016), application of oxidoreductase enzyme is according to the side electroactive catalysis product of biomolecules. One clear example, hydrogen peroxide (H_2O_2) which is subsequently cleaved into H^+ as electrochemical signal. Moreover this type of enzyme also requires the presence of coenzymes; for example : NAD^+, $NADP^+$, NADH, NADPH, ATP, FAD, FADH, which regenerates the enzyme to allow the subsequent reactions. Moreover, it is also distinguished between first, second and third generation in accordance to the electrochemical signal and coenzyme. Owing to the H_2O_2 as redox side product, the first generation employs dehydrogenase coenzyme in this following equation:

$$S + E - FAD \rightarrow E - FAD - S \rightarrow E - FADH_2 + P \ (1)$$

$$E - FADH_2 + O_2 \rightarrow E - FAD + H_2O_2 \ (2)$$

Subsequently, due to dehydrogenase reaction the NAD^+ and H^+ gradient is driven by this equation :

$$S + E + NAD^+ \rightarrow S - E - NAD^+ \rightarrow E + P + NADH + H^+ \ (1)$$

$$NADH \rightarrow NAD^+ + H^+ + 2e^- \ (2)$$

In contrast the second generation of enzymatic biosensor relies on oxidation (M_{Ox}) and reduction (M_{Red}) of mediator which drives the electron flow in this following equation:

$$S + E \ (ox) \rightarrow P + E \ (red) \ (1)$$

$$E \ (red) + 2\ M_{Ox} \rightarrow E \ (ox) + 2\ M_{Red} + 2H^+ \ (2)$$

$$2\ M_{Red} \rightarrow 2\ M_{Ox} + 2e^- \ (3)$$

On the other hand, direct electron transfer between enzyme and electrode is driven by redox polymer as signal propagation. Hence the third generation has not been implemented widely in analysis due to development process by integrating polymer science and nanotechnology.

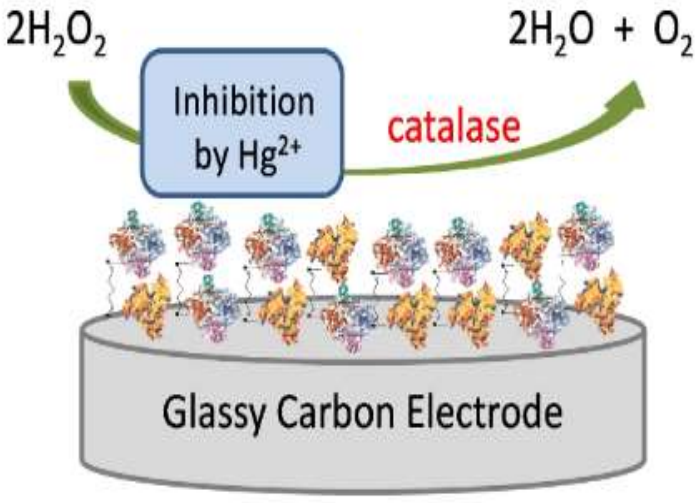

Figure 3 : Catalase inhibition by mercury (Hg2+) as amperometric detection of Hg (Elsebai *et al*. 2017)

Nevertheless, Elsebai *et al*. (2017) emphasized that enzyme inhibition is also relied as principle. One clear example amperometric measurement of mercury concentration was constructed by mercury (Hg) inhibition of catalase hydrolysis of hydrogen peroxide (H_2O_2) in glassy carbon electrode. In accordance to the electric current release by H_2O_2 presence as well as shrinking enzyme activity due to inhibition, greater concentration of mercury will drop the amperometric current. Therefore it was noted as percentage of inhibiton by this formula :

$$I\ (\%) = \frac{I_0 - I_i}{I_0}\ x\ 100\ \%$$

It is noted that I (%) is percent of inhibition, I_0 as initial current and I_i as inhibition current in certain Hg concentration.

Owing to the protein and enzymatic activity, Monteiro and Almeida (2019) emphasized the apo- enzyme form is the key of biosensor. Apo – enzyme is protein form of enzyme in which the catalytic activity is active. Moreover, the administration of prosthetic group as well as electron transfer agent is required to maintain enzymatic activity. In contrast, sensitive properties of enzyme particularly against temperature and ionic condition leads the denaturation of enzyme in which the bonds are broken. Hence, the integration of other methods is required which will results not only improving the specificity but also maintaining the enzymatic activity, for example ; nanoparticle and electroactive polymer enzyme immobilization.

Artigues *et al*. (2017) emphasized the amperometric parameters of enzymatic biosensor with glucose oxidase as example. In this system, anodic current alteration is a signal that represents the concentration product, which proportional to analyte (substrate) concentration stoichiometrically. Furthermore, in amperometric biosensor blocking of reductive species is required to prevent contamination of analyte. In short, amperometric biosensor requires the several types of immobilization agent for enzyme.

Figure 4 : Integration scheme of enzyme modified electrochemical biosensor (Pinyou *et al*. 2019)

Four major integration methods for enzyme immobilization and surface modifications are: functionalization, polymer modification, nanomaterials and protein engineering. Firstly, the polymer coating provides the cavity or pores as chemical interaction between enzyme and substrate as well as enzyme adsorption, notably electrospined nanofiber with high absorption efficiency. Secondly, large surface area and electrostatic interaction between enzyme and substrate of nanomaterials. Thirdly, protection of enzyme from environmental condition and the bond between enzyme, substrates and electrodes are generated by protein engineering (Pinyou *et al*. 2019).

Cyclic voltammetry (CV) is widely utilized to determine the redox properties of analyte as prerequisite of electroanalysis as both of cathodic reduction and anodic oxidation potential are detectable. In accordance to the enzymatic reaction, CV is widely applied in enzyme inhibition assay as the electroactive species is released during enzymatic reaction. In their research, Alpha glucosidase enzyme inhibition detection was performed by CV of p – Nitrophenol measurement (Mohiuddin *et al*. 2016). Consequently, voltammgram obtained the plot of the oxidative and reduction plot is obtained by voltammogram. Subsequently in accordance to Liu *et al*. 2017, the obtained

electrical potential from CV is implemented as range in differential pulse voltammetry (DPV) to measure the analyte concentration.

Application of enzyme as biosensor due to its specificity catalytic activity as molecular recognition element. Apart from this, enzyme as catalytic protein possesses certain binding activity which is regulated by side chain such as lysine (ε – amino group), cysteine (thiol group), aspartic and glutamic acid (carboxyl group) as well as the catalytic activity which is regulated by charged amino acid for example: arginine, lysine, histidine, tyrosine, threonine and serine. Apart from this, the election of oxidoreductase class enzyme is applied because this class release H_2O_2 as the side product of biomolecules oxidation. Subsequently this H_2O_2 emits H^+ which drives the electrochemical signal that corresponds the analyte concentration. Apart from this, covalent bonding formation in the self – assembled monolayer (SAM) leads strong binding over adsorption of enzyme which stabile immobilization. Owing to chemical bond properties of enzyme, a number of chemical methods which has been applied to stabilize enzyme by immobilization for example : Van der Waals forces, electrostatic and hydrophobic interactions (Nguyen *et al*. 2019).

2.2.1. Immobilization system

Owing to degradability and risks of enzyme against environmental factors such as: temperature, pH, ion concentration and denaturation; enzyme immobilization is required to maintain the stability and reliability. A number of goals of enzyme immobilization are: facilitate biocatalyst recovery, modulating selectivity – specificity and improve resistance against inhibitor. As a result of industrial and lab demand as well as environmental public policy, various materials has been employed as enzyme immobilization carrier particularly polymers, nanoparticles (metal or non-metal) and metal organic frameworks. A broad range of principle within physical and chemical has been employed as principle in enzyme immobilization for instance: covalent attachment, cross-linking, adsorption, encapsulation and entrapment. Meanwhile a number of protein properties are elected for immobilization design for example: conformational flexibility, isoelectric point, surface functional groups, glycosylation, immobilization stability, hydrophobic – hydrophilic regions and additives (Liu *et al*. 2021).

Apart from this entrapment method relies on capture of enzyme by a matrix cross – linked network. Consequently, substrate is also capable to penetrate the matrix for subsequent enzymatic reaction without enzyme release to outside environment. A crucial criteria of enzyme entrapment matrix is the capability of water absorption and swelling due to its hydrophilicity. One clear example, hydrogel styrylpyridine gelan gum for immobilization of catalase. (Monier *et al*. 2020). In addition, chitosan is also capable to conduct entrapment because of its hydrophilicity of amine groups. Hence chitosan is utilized to immobilized glucose oxidase (GOx) for Au – Ti electrode (Lipinska *et al*. 2021).

Covalent immobilization relies on covalent bond between enzyme carrier and non-active site amino group of enzymes as well as it regulates accessibility of active center and uniform distribution. Consequently, enzyme release from its carrier is prevented as the presence of hydrophobic and Van der Waals interaction is nullified. Moreover, enzyme degradation by environmental factors is diminished (Wang *et al*. 2020).

Moreover, cross – linker like glutaraldehyde is also utilized in covalent attachment enzyme immobilization such as trypsin into non-woven chitosan (Kim and Lee 2019). Owing to covalent bond, cross linker forms reversible Schiff base between amino and aldehyde group. A number of factors are influential in covalent immobilization of enzyme for example: buffer solution, pH, and incubation time and trypsin concentration. In addition, temperature is also influential in storage and activity stability.

In accordance to various physico – chemical low force interactions, for example hydrogen bonding, ionic or mixed adsorption enzyme immobilization has been developed. The advantage of this method are low cost and retention of catalytic activity. In contrast, the major weaknesses are rapid decrease of catalytic properties, alteration of enzyme and weak interaction between enzyme and carrier. A number of functional groups are relied for adsorption immobilization notably: hydroxyl, amine and carbonyl. One clear example PCL–chitosan composite was researched for adsorptive tyrosinase immobilization for bisphenol – A degradation (Zdarta *et al*. 2020).

In recent times, enzyme immobilization has been implemented in electrochemical biosensor to improve its selectivity and specificity. Owing to specific reaction and oxidoreductase property, hydrolysis of certain substrate with an enzyme will generate the

electron. Subsequently this electron flow will emerge as electrical current. Hence, enzyme immobilization into electrode is applicable by employing suitable matrix to prevent leak (Sharma *et al*. 2017).

2.3. Uricase (UOx) Enzyme Based Biosensor

Glassy carbon electrode (GCE) was used for UOx based electrochemical biosensor. In the research of Omar *et al*. (2016), graphene oxide (GO) was applied to modify GCE both of improves its selectivity and surface area as well as for UOx immobilization agent. Hence, the LoD achieved 3.45 uM in amperometric measurement. Meanwhile in the research of Yan *et al*. (2020), nanocube cuprous oxide – ferrocene was utilized to modify GCE as both of UOx immobilization agent and electron mediator – selectivity. Hence it achieved LoD 0.0596 μM.

Indium tin oxide (ITO) was constructed as UOx electrochemical enzymatic biosensor in the research of Verma *et al*. (2019) which also modified with Au – rGO (gold – reduced Graphene Oxide) nanocomposites. In this system, ITO was firstly coated with Au – rGO nanocomposite before covalent immobilization of UA with EDC – NHS crosslinker. It was also noted that nanocomposites coating acted to elevate surface area and enzyme immobilization agent. In addition, the LoD was 7.32 μM.

Apart from this, flow system in electrode was researched by Tvorynska *et al*. (2021) as UOx MCM41 mini reactor electrode. In this system, sample which contains UA was flowed to glass cell. Hence, sample was flowed firstly to enzymatic reactor than detection took place in tubular detector. Owing to 3 electrode system, tubular detector roled as working electrode while both of counter and reference electrode was placed in the edge. Subsequently, analysis was terminated by flowing the waste from the system. In this system, LoD was 18.5 μM.

2.3.1. Uricase (UOx) enzyme

Uricase (UOx) is oxidoreductase enzyme class which catalyzes UA into hydrogen peroxide and 5-hydroxyurate which subsequently transforms into allantoin. In accordance to enzyme nomenclature UOx is noted as 1.7.3.3 which notes as oxidoreductase (1), reacts with other nitrogenous compound (1.7), utilize oxygen as acceptor (1.7.3) and urate

hydroxylase independent factor (1.7.3.3) (Kim *et al*. 2016). Owing to UA as oxidation product of purine, UOx enzyme has been found in a number of microorganisms notably : *Candida* sp. and *Aspergillus niger* for fungi and *Arthrobacter globiformis* , *Bacillus fastidiosus* and *Comamonas* sp. for bacteria. As a result of broad range of source, a number of enzyme optimization parameters for UOx is different for example optimal pH, isoelectric point (pI), enzymatic activity, molecular mass and stability (Tvorynska *et al*. 2021).

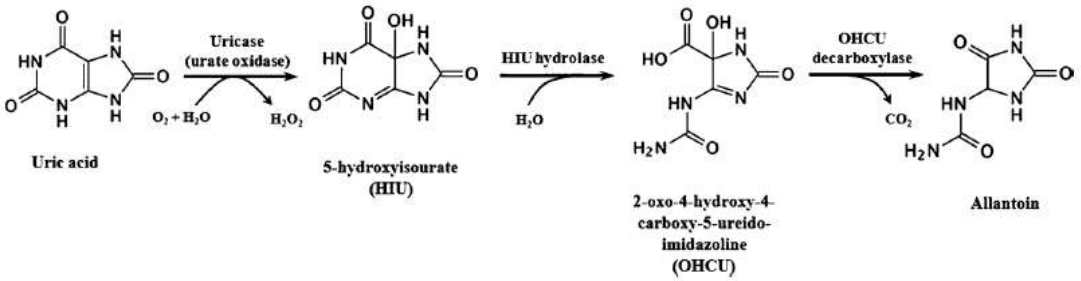

Figure 5 : Schematic UA oxidation by UOx enzyme (Mirzaeinia *et al*. 2020)

One clear example, UOx from *Candida sp.* is widely used in various experiment as it does not require any cofactor in enzymatic oxidation. Moreover, it shares significant amino acid sequences similarity with other organism UOx for example : *Aspergillus flavus* 49 % , mammalian UOx 33 % , *Bacillus* sp. UOx 22 % and *Glycine max* UOx 33 %. Meanwhile optimum pH is 8.5 with optimum temperature 40ºC (Liu *et al*. 2011). In addition, isoelectric point (pI) of *Candida* sp. UOx is 5.6 with stability at Borate buffer pH 8.5 to 9.5. Meanwhile *Candida* sp. UOx is strongly inhibited by Hg^{2+}, Cu^{2+}, Ba^{2+} and Fe^{3+} (Liu *et al*. 1994).

Apart from this UOx enzyme is also found in vertebrates. One clear example Zebrafish (*Danio rerio*) UOx represents the evolutionary of uricolytic pathway in hominoids as inactivation. Owing to genomic and proteomic comparison between zebrafish and *Macaca fascicularis*, space slice mutation of phenylalanine to serine drives the inactivation of urate degradation pathway in hominoids. Consequently, this mutation drives shrinkage of catalytic efficiency that triggers further elevation of in vivo UA

concentration. In contrast, urotelic vertebrates particularly birds and reptiles conserves UOx genes by the absence of inactivating mutations (Marchetti *et al*. 2016).

2.3.2. SPCE based UOx biosensor

Owing to analytical reliability which is focused to electro analytical chemistry, miniaturization of system is required to support its reliability. One clear example, screen printed electrode is a current emerging analytical system which resemble the general electrode principle consists of working electrode (WE), counter electrode (CE) and reference electrode (RE). Firstly for WE it requires conductive inert carbonaceous materials for example : carbon black, carbon nanotube and graphene. Meanwhile RE requires fixed stable potential such as Ag and AgCl. In addition, CE roles to close the current circuit of electrochemical system by employing inert materials notable Pt or Au (Cinti *et al*. 2017, Antuna – Jimenez *et al*. 2020 and Gonzalez – Sanchez *et al*. 2018).

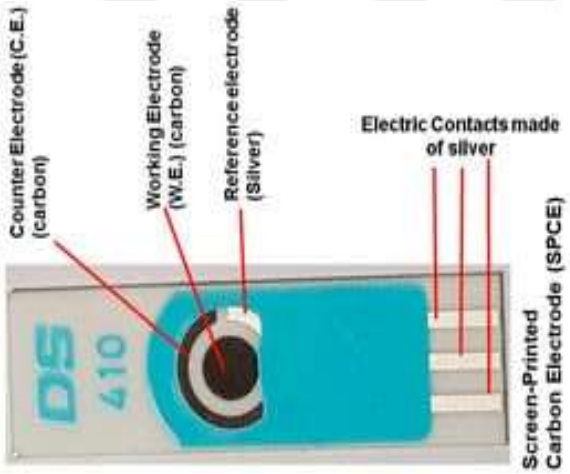

Figure 6 : Schematic of Screen Printed Carbon Electrode (Krampa *et al*. 2017)

A broad range of carbon graphite derived materials has been utilized as working electrode (WE) which is classified by its texture and structures for example : adsorptive carbon, carbon nanotube and graphene oxide. In accordance to sp^2 hybridization and presence of hexagonal layers in carbon atoms, the subsequent formation of intercalated covalent and pore form which leads to higher specific surface area. Owing to Freundlich

and Langmuir adsorption isomer against 2,4-D herbicide, it was noted from highest to lowest was carbon nanotube, adsorptive carbon and graphene oxide. Apart from this the consecutive order from highest to lowest was also exhibited for current intensity of 2,4-D herbicide DPV analysis (Kusmierek *et al*. 2021).

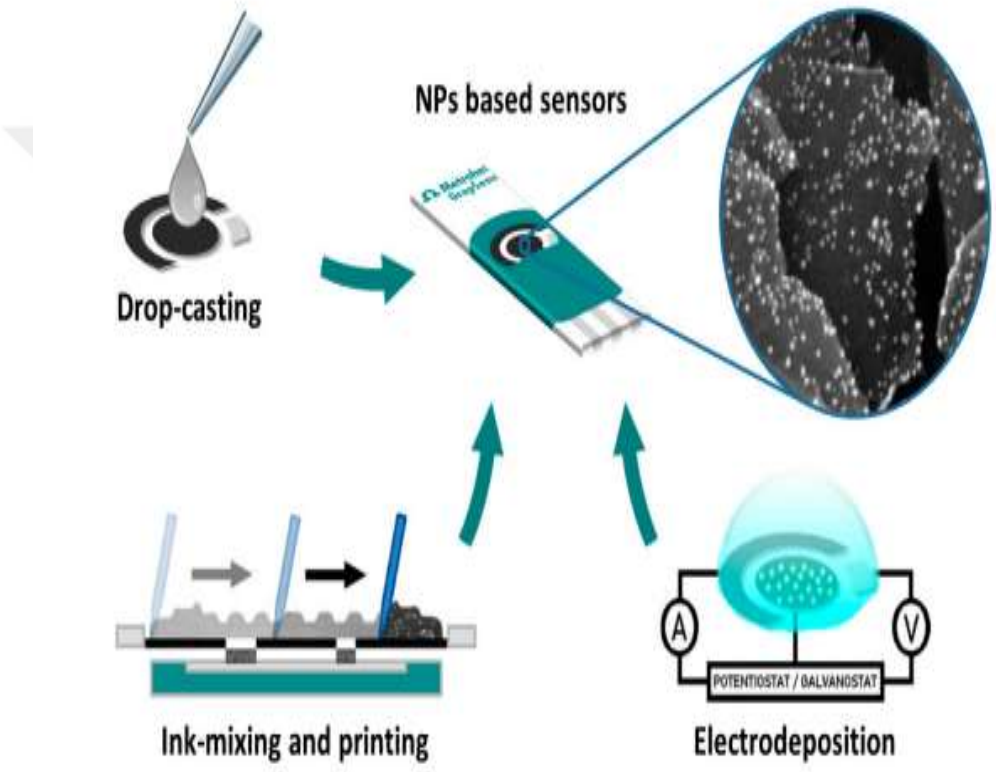

Figure 7 : Metal modification of screen printed carbon electrode (Antuna – Jimenez et al. 2020)

In the review of Antuna – Jimenez *et al*. (2020), it was emphasized that SPCE is modifiable by metal to improve its conductivity. Four major methods in metal modifications of working electrode are : electrodeposition, ink mixing – printing, metal nanoparticle modification and dropcasting. A number of common metals for modifications for example : copper, nickel, gold, silver, platinum and bismuth. Ink mixing – printing process is initiated by the mixture of conductive carbonous material ink with

metal nanoparticles notably : gold, silver, platinum and iridium. Subsequently metal modified carbon working electrode exhibits higher analytical reliability by interconnection of metal – carbon particles, higher electron transfer and lower resistance. Drop casting method is the easiest as it only requires the optimization of final dropcasted concentration into WE by relying on metal nanoparticle concentration in dispersion and drop size. In contrast, agglomeration is the only major weakness as metal nanoparticle aggregates in drying with microparticulated appearance. Consequently, catalytic performance and subsequent conductivity is improved by the metal – carbon center improvement of electroactive area. One of the most advanced methods is electrodeposition of metal nanoparticles which relies on reduction of oxidized species that tailor – made metal nanoparticles is obtained by fixed potential or current. A number of usual salts for example : $AgNO_3$ (silver nanoparticle), $HAuCl_4$ and $AuCl_3$ (gold nanoparticle) and $CoCl_2$ (cobalt nanoparticle).

In correlation to carbon microporosity as current approach in electrochemical analytical reliability, it is crucial as the less than 1 nm diameter enables selectivity of tiny analytes particularly protons in broad infra. Consequently, a number of advanced carbon has been developed to improve its microporosity for example : tailored microporous carbon, nano dot carbon, pyrolytically produced carbon and heterocarbon. Owing to pH and ionic alteration in electrochemical analysis, capacitive switching is enabled by microporous nanocarbon. Subsequently voltammetric impedance pH response is also developed as current signal output. (Hernandez *et al*. 2017).

Screen – printed carbon electrode (SPCE) enables miniaturization of electrochemical biosensing in various analyte such as UA. Subsequently, this SPCE with graphite carbon is proper to be integrated with polymer such as 4 – amino – salicylic acid (4 – ASA) as both of coating and UOx immobilization agent as well as Prussian blue mediator. Consequently, mediator will improve the sensitivity. Hence the selectivity is elevated to analyze UA with LoD 3.5 μM for UA detection in urine (da Cruz *et al*. 2017).

In addition, cationic polymer is also applicable for SPCE coating to improve selectivity of enzymatic UA detection. One clear example: PVA – SbQ (poly (vinyl alcohol) N – methyl – 4(4'-formylstyryl) pyridinium methosulfate acetal) was implemented by RoyChoudhury *et al*. (2018) to modify SPCE. Moreover, cationic

polymer was also capable to entrap the electron mediator such as Ferrocene carboxylic acid (Fca). Hence UOx was immobilized in this polymer and the electrochemical system was capable to detect UA from sweat and wound band by CV. Subsequently, the LoD was 12 μM with sample recovery 104 – 107 %.

Apart from this, SPCE was also applicable for enzyme immobilization with the absent of polymer while mediator presence. In the research of Piermarini *et al*. (2013), UOx enzyme was immobilized directly into SPCE by the assist of glutaraldehyde as crosslinker. Moreover, Prussian blue was applied as mediator. Hence, it achieved LoD as 10 μM for blood serum UA detection.

Owing to practical application and manufacturing, Jirakunakorn *et al*. (2020) fabricated the UOx biosensor as homemade SPCE. Subsequently, SPCE was coated with Prussian Blue and modified with chitosan - graphene composite cryogel for UOx enzyme immobilization. Hence, it achieved LoD as 2.5 μM in the Flow Injection Amperometry analysis.

2.4. Electrospinning

Electrospinning the recent growing manufacturing method of polymer nanocomposite has taken broad attention as its capability to accommodate certain crucial properties such as: fibrous structure, mechanical properties, biocompatibility and biodegradation. Owing to the principle, electrospinning employs four major parts: syringe containing polymer solution, metallic needle, power supply and metallic collector. As a result of electrical flow into polymer by passing through metallic needle, subsequent instability of polymer solution by induction alteration is happened. Simultaneously, surface tension opposing force is also generated which subsequently drives the reciprocal repulsion and polymer flow in the electric field direction. Furthermore, deformation of spherical droplet is led by conical shape generates the subsequent ultrafine nanofiber in metallic collector. Finally, nanofiber is generated by cohesive forces with whipping motion which enables sliding and stretching of each polymer chains (Haider *et al*. 2018).

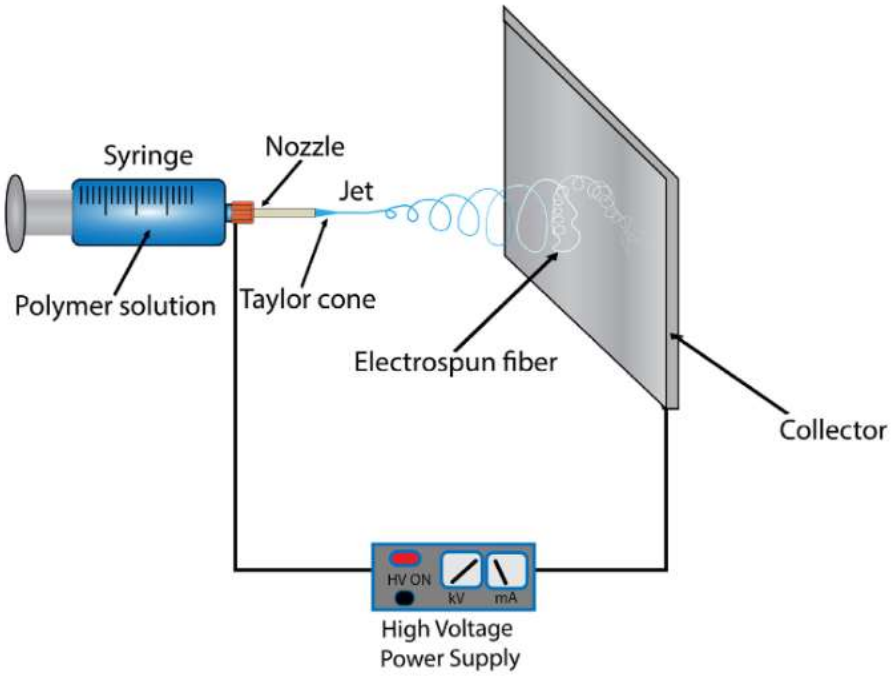

Figure 8 : Work scheme of electrospinning (Hussain *et al*. 2021)

Manipulation of a number crucial parameters such as: alternating current, applied voltage, alternating current and incorporation of porous materials will modify the fiber homogeneity, diameter, morphology and porosity. Moreover, size and morphology of electrospin fibers is also controlled by electrospinning setup parameters, polymer solution properties, and ambient conditions. Also, tiny diameter fiber which is less than 1 um to nanometers is fabricated efficiently by the variation of polymer concentration, feeding rate and applied voltage. In contrast, low viscosity polymer mixture will generate fiber with beads with non-uniform length (Hussain *et al*. 2021).

Major crucial parameters in electrospinning are divided into 3 groups: solution, processing and ambient parameters. Firstly, solution parameters consist of solvent volatility, polymer concentration, viscosity and molecular – weight branching. It is widely noted that higher polymer concentration with higher viscosity leads increase of fiber diameter and electrospinability. In addition, solvent volatility determines wet or dry electrospinning as well as linear polymer facilitates entanglement. Secondly processing parameters for example: collector type, spinning distance, applied voltage and flow rate

determines the fiber alignment as well as beading and continuity of fiber. Thirdly ambient parameters for instance: humidity, temperature and air flow which lead solvent evaporation rate with subsequent stability of polymer fiber. (Angel *et al*. 2022).

In accordance to solvent in polymer electrospinning, miscibility is important factor in polymer and its solvent mixture election. It is widely noted that the blend with the absence of separation phase enables the mixture for further electrospinning. In contrast, similar viscosity with polymer immiscibility in solvents generate subsequent electrospinned inner core and outer sheath layer of nanofiber (Voniatis *et al*. 2021).

2.5. PCL – PEI

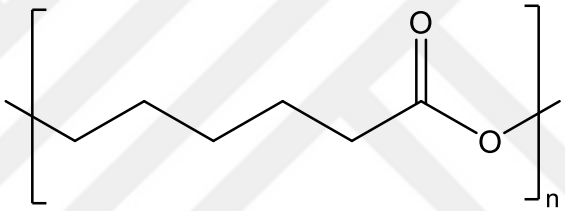

Figure 9 : Chemical structure of PCL (Das *et al*. 2020)

Owing to the existence of carboxyl and alkyl group of polyester notably PCL, biocompatibility, biodegradability as well as sufficient mechanical strength are exhibited. Moreover, the oxygen electron of PCL carboxyl group is capable to form hydrogen bond with another polar polymer such as: N-H and O-H. Subsequently, ester bonds of PCL are breakable by the addition of formic acid during electrospinning in mixing with other polar polymers (Das *et al*. 2020).

In the research of Wei *et al*. (2020) it was emphasized that PCL is reliable as nanofibers and nanoparticle carriers by relying its hydrophobic core as core of micelle environment. Apart from this, Baker *et al*. (2016) carried out Atomic Force Microscopy analysis which confirmed a number of distinct mechanical properties of PCL notably elasticity and mechanical strength. Furthermore, electrospin PCL exhibited strong anchoring capacity with fiber diameter 440 to 1040 nm. In addition, the molecular weight of PCL is MW = 120,000 – 300,000 gram/ mol with consecutive maximum strain values

40 %, 100 % and 200 % for 10 wt %, 12 wt % and 14 wt % of PCL. Additionally, incremental stress – strain curves showed total tensile modus 62 MPa and elastic tensile modus 53 MPa.

Owing to PCL degradability, Nguyen *et al*. (2022) reported that PCL based nanofiber prosthesis drives the fibronectin alteration as Atomic Force Microscopy (AFM) result. In terms of mechanical and thermal properties alteration during PCL degradation in fibronectin tissue, Mn and Mw decreased while Tm increased. Moreover, this degradation process is in accordance to semi crystalline biodegradable polymers at less amorphous zone level with greater crystallinity. Furthermore, in physiological conditions PCL degradation took place by the generation of –COOH and –OH group as a result of macromolecular chains scission.

A number of study reported the hydrophobicity of PCL which requires the alteration and improvement of hydrophilicity by the addition of other polar polymers. One clear example is ionic pH responsive polymer names Polyacrylic Acid (PAA) that functioned as ion donor. Apart from these polar polymers which possesses hydrogen bond has been also utilized to modify PCL and upgrades its hydrophilicity for example: Polyvinyl alcohol (PVA), polyethylene glycol (PEG) and polylactic acid (PLA) (Huang *et al*. 2021).

Meanwhile, PCL is also capable to be integrated as polymer mixture with protein or nitrogenous charged polymer in electrospinning to improve its hydrophilicity. One clear example, collagen is electrospinned as biocompatibility scaffold in artemisinin delivery by Huo *et al*. (2021). Also, Bigham *et al*. (2021) reported the use of silk fibroin as composite with PCL for bone tissue regeneration. Another example, Wang *et al*. (2019) reported that the improvement of nanocarrier capacity was achieved by the construction of PCL – PEI nanocomposite as PEI drove the higher hydrophilicity.

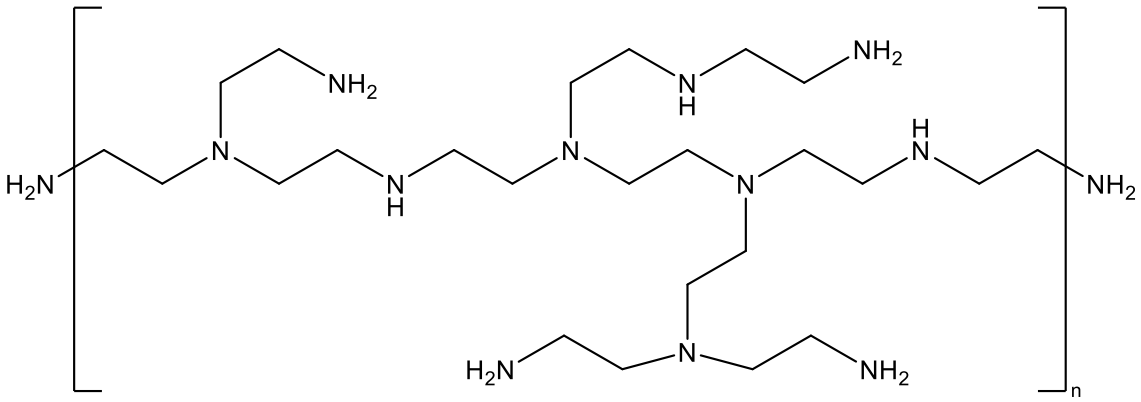

Figure 10 : The Structure of PEI (Miyazaki *et al*. 2017)

PEI is polymerized by its ethylene imine monomer which consist of ethylene and imine group. Owing to the polarity of imine group, interlayer electrostatic interaction is indicated by the existence of several following dissociation constants (pKa): $pKa_{1:}$ 9.0 (primary amine), pKa_2 : 8.0 (secondary amine) , pKa_3 : 6 – 7 (tertiary amine). Subsequently, most of the amine groups are protonated at pH between 5 and 6. In addition PEI is capable to form hydrogen bonding by using its imine group (Miyazaki *et al*. 2017).

As a polyelectrolyte, PEI exhibits distinct properties as charge is bear along the backbone unlike other polyelectrolytes which bears in side chain. Consequently, protonation of all amines drives the diminishing of Bjerrum length as well as Coulombic potential which consequently increase its protonation level. Meanwhile, protonated fraction α alters from 0.2 in pH > 7 to 0.9 in pH below 3. Owing to solubility, PEI dissolves difficultly in alkali solution while unprotonated PEI has slight application (Gallops *et al*. 2019).

Previously Argaman *et al*. (2021) researched the PEI as stabilizing compound in Aldehyde Dehydrogenase (ALDH) immobilization into clay. Owing to branched positive charge of PEI, it was elected to create bridge between negative charged clay and protein. Furthermore, it is capable to maintain enzymatic activity during immobilization as a result of electrostatic interaction between PEI and protein which creates water – saturated casing. Consequently, PEI has been employed in various biotechnology methods for example: protein precipitation, immobilization agent, delivering vector of oligonucleotides and plasmids, thermal stabilizer of solution on solid surfaces.

Galliani *et al*. (2019) emphasized that pure PEI exhibit positive charge by its zeta potential was + 42.7 mV with hydrodynamic diameter 279 nm. Subsequently, positive value of zeta potential was retained by PEI during further immobilization of superoxide dismutase (SOD) enzyme which zeta potential was + 38 mV and encapsulation efficiency was 63 % and activity yield was 29 %. Moreover, addition of bovine serum albumin (BSA) also elevated PEI zeta potential to + 48 mV. Hence, cationic polymer delivery of SOD was created by relying on the principle of proton sponge capability which lead endocytosis – endosomal escape.

2.6. Aim of Thesis

UA is crucial molecule to detect uricemia either hyperuricemia or hypouricemia diseases. Hence it is important to conduct research for the development of UA biosensor system. In practice, there are colorimetric, chromatographic, spectrophotometric and biosensor-based methods for UA determination. However, there is still an important need for the determination of UA, especially selective and easy-to-use systems. In this thesis, the preparation of screen-printed electrodes containing membranes prepared by electrospinning, the immobilization of UOx enzyme and its use as a voltammetric UA biosensor for the selective and sensitive determination of UA are available.

3. MATERIALS AND METHODS

3.1. Materials Used in Thesis

In the content of this study, materials used in research were given Table 3.1.

Table 3.1 : Materials used in research

Material	Properties	Manufacturer
Uric Acid (UA)	>99 %	Acros Organics
Uricase (UOx) Enzyme	>99 %	Sigma Aldrich
Polycaprolactone (PCL)	Mn 80,000	Aldrich
Polyethylene Imine (PEI)	Mw 10,000 99 %	Alfa Aesar
Dimetheyl Formamide (DMF)	>99 %	IsoLab
Chloroform ($CHCl_3$)	>99 %	IsoLab
Methylene Blue (MB)	>99%	Carlo Erba
Glutaraldehyde (GA)	25 % in aqueous	Sigma Aldrich
Dopamine	>99 %	Alfa Aesar
Glucose	>99 %	Merck
Lactic Acid	>99 %	Sigma Aldrich
Urea	>99%	Merck
Ascorbic Acid	>99 %	Sigma Aldrich
CdSe QD SPCE	WE : Carbon – QD CdSe CE : Platinum (Pt) RE : Silver (Ag)	Dropsens

3.2. Instruments Used in Thesis

In the content of this study, instruments used in research were given Table 3.2.

Table 3.2 : Instruments used in research

Instrument (Manufacturer)	Institution / Organization
Iviumstat Electrochemical Device (Ivium)	Inonu University, Lab Biochemistry – Biomaterials, Department of Chemistry, Faculty of Science and Literature
Electrospinning Device (NS1 Nanospinner)	Inonu University, Lab Biochemistry – Biomaterials, Department of Chemistry, Faculty of Science and Literature

UV – Vis Spectrophotometer (Shimadzu)	Inonu University, Lab Biochemistry – Biomaterials, Department of Chemistry, Faculty of Science and Literature
Water Bath (Wise Bath)	Inonu University, Lab Biochemistry – Biomaterials, Department of Chemistry, Faculty of Science and Literature
Electronic Balance (Sartorius)	Inonu University, Lab Biochemistry – Biomaterials, Department of Chemistry, Faculty of Science and Literature
FTIR (Perkin Elmer)	Inonu University, Lab Physical Chemistry, Department of Chemistry, Faculty of Science and Literature
Contact Angle	Inonu University, Lab Physical Chemistry, Department of Chemistry, Faculty of Science and Literature
XRD	Inonu University, Integrated Laboratory IBTAM
EDX	Inonu University, Integrated Laboratory IBTAM
SEM	Inonu University, Integrated Laboratory IBTAM

3.3.Methods Applied in Thesis

3.3.1 PCL – PEI Electrospinning

PCL 10 % and PEI 7.5 % was mixed in Dimethylformamide (DMF) and Chloroform ($CHCl_3$) 1:3 for overnight mixture. Subsequently electrospinning was carried out for this mixture with following parameters: Applied voltage 15 kV, Flow rate 1 mL per hour, distance 15 cm and spinning time 10 minutes. Electrospinned PCL – PEI nanofiber was divided into two groups: without and with methylene blue 0.05 mM (Wang *et al*. 2019 with modification).

3.3.2. Enzyme Immobilization

Electrospinned PCL 10% - PEI 7.5% was cut 1 x 1 cm for treatment with 0.1 % Glutaraldehyde (GA) in 37^{o}C for 1 hour. Subsequently the cut membrane was washed with 0.05 M PBS pH 7.4 to remove the excess GA before incubation overnight with 4 U / mL UOx enzyme (Zaak *et al*. 2017 and Zdarta *et al*. 2020).

3.3.3. Enzyme Assay

UOx activity was tested by UV Vis spectrophotometry in 293 nm in accordance to the UA absorbance with substrate incubation at 10 minutes in 40^{o}C (Mirzaeinia *et al*. 2020).

3.3.4. Polymer Characterization

Polymer, before and after immobilization were scanned by FTIR in spectral range 4000 – 400 cm^{-1} at 4 cm^{-1} spectral resolution. Thereafter, spectra were recorded (Kowalczuk and Pitucha 2019).

SEM was carried out in accordance to the method of (Ding *et al*. 2021), by applying magnifications 5000 and 20.000 times with 20 kV potential. Polymer fiber both of before and after immobilization are scanned. Samples were also coated with gold and palladium nanoparticle.

EDX was carried out with 3 mA , 20 kV applied voltage with 125 eV Bruker detector in 400 μm analysis area (Hernandez – Ibanez *et al*. 2022).

XRD analysis was carried out in CuKα radiation source with 2 θ range from 10 to 90^{o} , kV , wavelength 1.54 Å and scan speed 2^{o} per minute (Degorska *et al*. 2021).

3.3.4.a. Contact Angle

Contact angle measurement was carried out with method of Dufay *et al*. (2021) which utilized PCL based nanofiber. Firstly, polymer film was dropped by 3 μL and incubated 30 seconds to measure the contact angle optically and digitally by image processing. Measurements were carried out in 25^{o}C with triplicate.

3.3.4.b. Swelling

Swelling behavior was tested in accordance to the method of Le *et al*. (2022). Firstly, polymer with size 1 x 1 cm was soaked at PBS buffer pH 7.4 in 37^{o}C for 15 minutes in one hour. Thereafter excess water was absorbed by tissue and soaked polymer is weighed. Finally, it was calculated with equation below, Wo is initial weight while Wt is weight after soaking.

$$Water\ uptake\ (\%) = \frac{Wt - Wo}{Wo}\ x\ 100\ \%$$

3.3.5. Voltammetric Method

3.3.5.a. CV of $K_3[Fe(CN)_6]$

CV of QD SPCE (CdSe) was performed in 5 mM $K_3[Fe(CN)_6]$ for both of Bare QD SPCE, PCL/PEI/ UOx/QD SPCE and PCL/PEI/MB/UOx/QD SPCE with scan rate 10 to 100 mV per s. Thereafter linearity relationship was plotted between square root of scan rate (x) and peak current (y) which consisted of Cathode peak current and Anode peak current separately. By employing this method, the usability of electrode was examined (Aoun 2017). Furthermore, Randles – Sevcik equation was utilized to obtain electroactive area (A) and Ipa/Ipc (Peak current anode and cathode ratio) from the peak (Kanso *et al*. 2017).

3.3.5.b. DPV Standardization of UA

Both of PCL/PEI/ UOx/QD SPCE and PCL/PEI/MB/UOx/QD SPCE were utilized for DPV of UOx solution in 0.05 M PBS pH 7.4 between 5 and 52 µM concentration with standard addition. DPV was carried out with baseline subtraction, which employed parameters : E start : - 0.1 V, E end = 0.8 V , Pulse time 50 ms , pulse amplitude 30 mV, E step 10 mV and scan rate 50 mV per s. Also, pretreatment was carried out for 3 minutes due to enzymatic reaction. Meanwhile, linear for DPV curve relationship was plotted as I peak current (in µA) for y and analyte concentration (in µM) as x (Merlos Rodrigo *et al*. 2017 and Gonzalez – Costas *et al*. 2020).

3.3.5.c. Storage Stability Test

Storage stability test was carried out in accordance to the method of Topsoy *et al*. (2022) and Marquitan *et al*. (2020) with modification by utilizing 30 µM UA (median concentration) in DPV measurement once a week in a month.

3.3.5.d. Electrochemical Impedance Spectroscopy

Electrochemical Impedance Spectroscopy (EIS) was carried out in accordance to the method of Castano – Guerrero *et al*. (2021) and Riedel *et al*. (2017) which involved frequency range 0.01 Hz – 100 kHz ; value per decade 10 , number of frequency 50, amplitude 10 mV and constant potential start at 0.2 Volt.

3. 3.5.e. Interference Test

Interference test was carried out in accordance to the method of Wang *et al*. (2021) with modification. UA 30 μM was measured simultaneously with the mixture of interference which consisted of Lactic Acid 250 μM, Glucose 1 mM, Ascorbic Acid (AA) 250 μM, Dopamine 10 μM and urea 250 μM.

4. RESULTS

4.1. Characterization of PCL/PEI nanofibers

4.1.1 Surface morphology

The surface morphology and diameter of the PCL/PEI nanofibers was confirmed by SEM analysis before and after the enzyme immobilization process. The nanofibers were prepared at 10%, 7.5% and 5% PEI by weight of PCL concentration. From the results obtained, it was found that the PCL/5%PEI solution did not produce a uniform nanofiber without beads. In contrast, PCL/10%PEI showed bead structure nanofibers, owing to the cationic property of PEI that drives solution conductivity. As seen, PCL/7.5%PEI nanofibers were found that the nanofibers had almost the same diameter, positioned randomly, smooth and bead-free. Therefore, PCL/7.5%PEI nanofibers were chosen for UOx immobilization (Figure 4.1A). Also, the diameter of the PCL/7.5%PEI nanofibers was in the range of 150–400 nm. SEM images of UOx immobilized PCL/PEI nanofibers were given in Figure 4.1B. After immobilization, the structures of the nanofibers did not change and the average diameters were around 400–600 nm. The reason for the increase in diameter of nanofibers after immobilization can be explained by the amount of immobilized enzyme on the surface (Mirzaei *et al*. 2020).

In addition, the SEM images in Figure 4.2A-B show that the PCL/PEI/MB nanofibers have a fibrous structure with a fiber diameter between 300-500 nm, and the fibers are long, thin and smooth surfaced. On the other hand, PCL/PEI/MB/UOx nanofibers exhibited a bead-free, randomly oriented, continuous and rougher structure with a diameter of about 500-600 nm (Figure 4.2.C, D). The above-mentioned results indicate that UOx was successfully immobilized on the whole PCL/PEI/MB surface.

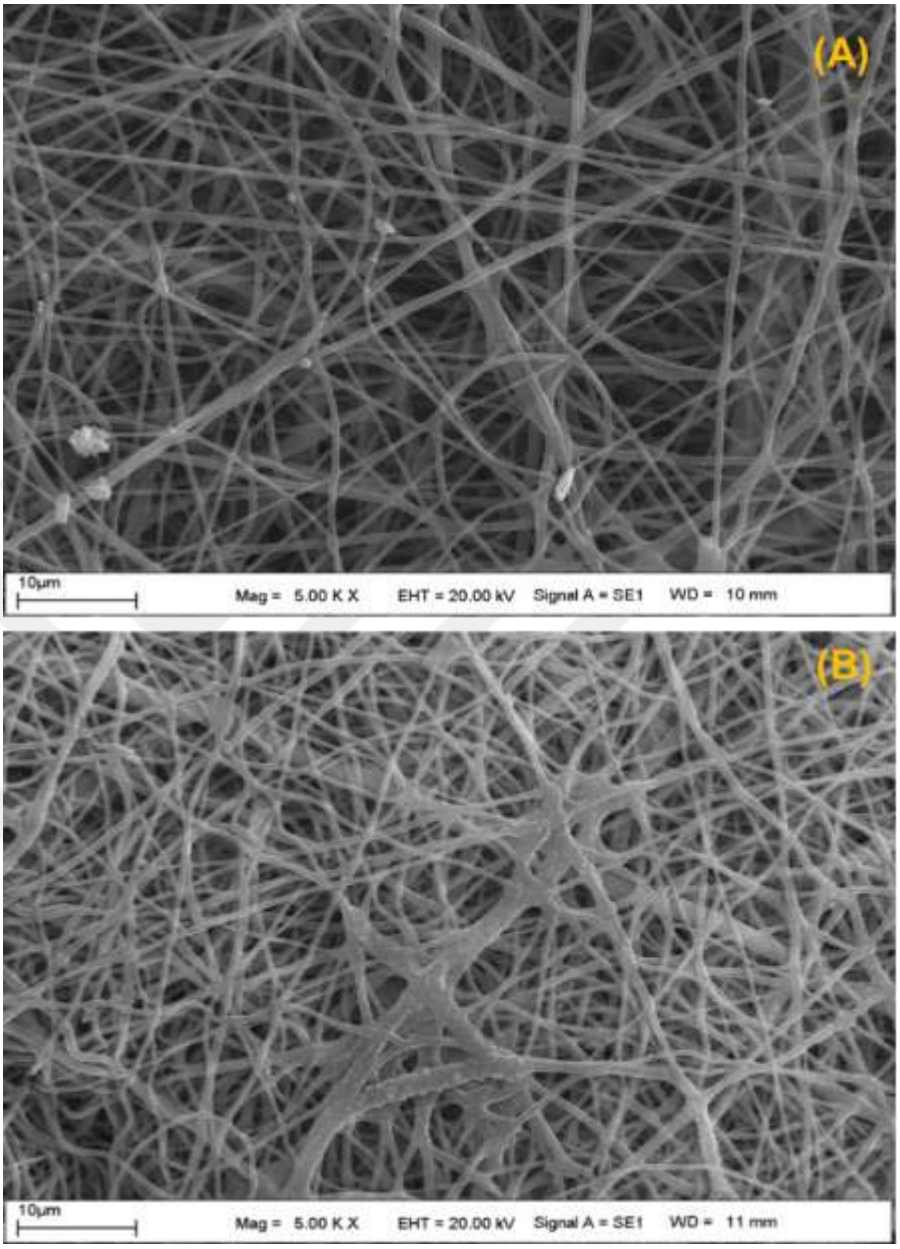

Figure 4.1 : SEM images of (A) PCL/PEI, and (B) PCL/PEI/UOx nanofibers

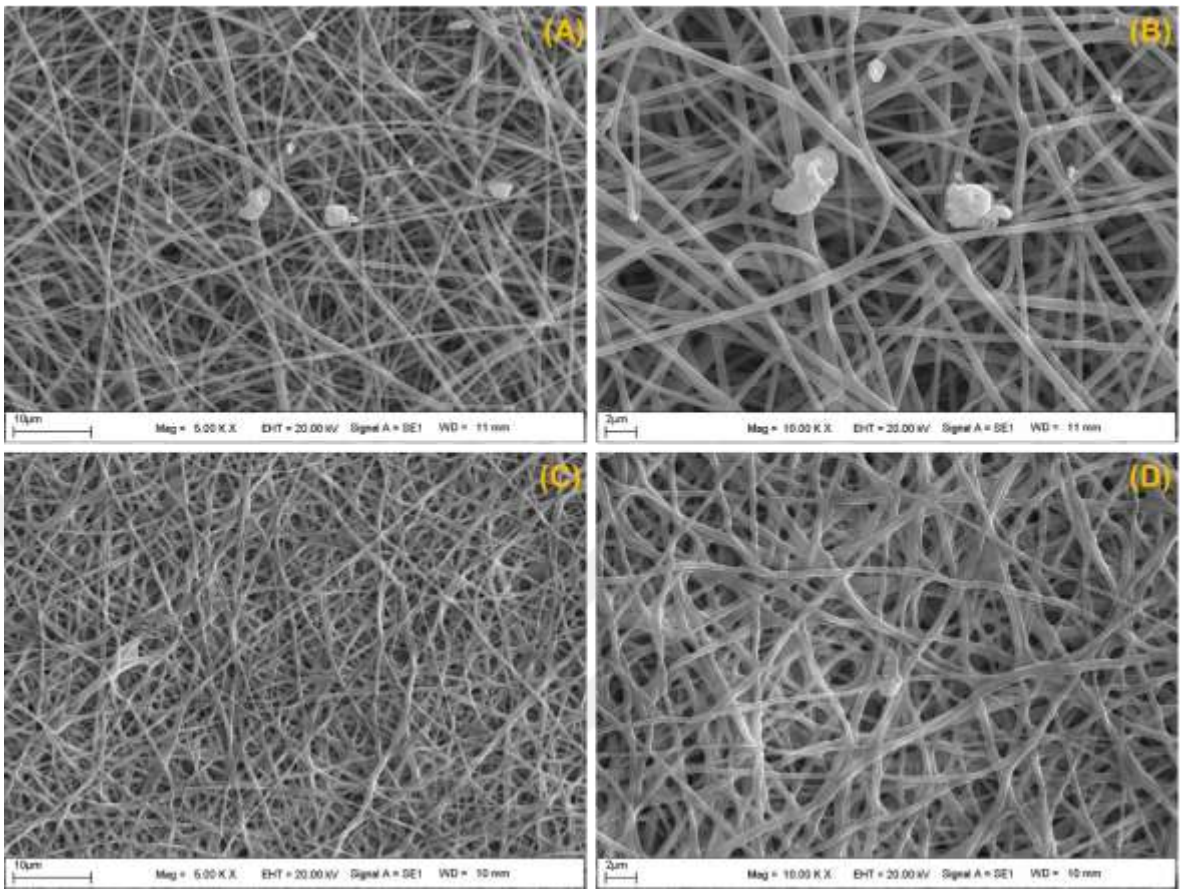

Figure 4.2 : SEM images of (A, B) PCL/PEI/MB, and (C, D) PCL/PEI/MB/UOx nanofibers at different magnifications.

4.1.2. FTIR analysis

FTIR spectra of pure PCL, pure PEI, PCL/PEI nanofibers, PCL/PEI/UOx nanofibers is displayed in Figure 4.3. The FTIR spectrum of pure PCL shows 2945 cm^{-1} (asymmetric $–CH_2$ stretch), 2886 cm^{-1} (symmetric $–CH_2$ stretch), 1724 cm^{-1} (carbonyl stretch), 1293 cm^{-1} (C–O and C–C stretching) and 1162 cm^{-1} (symmetric C–O–C stretching) bands. Pure PEI exhibits wideband N–H stretching vibrations at 3500 cm^{-1} and 2803–2930 cm^{-1} which represented aliphatic C–H vibrations. In addition, N–H vibrations of primary and secondary amino groups is indicated by two strong bands at 1594 cm^{-1} and 1448 $cm^{-1,}$ respectively. Meanwhile, the peaks at 1306 cm^{-1} and 1047–1120 cm^{-1} are associated with C–N peak stretching (Decarpigny *et al*. 2021). For the PCL/PEI

nanofibers, the characteristic peaks are observed in corresponding to the C–H stretching vibrations at 2942 and 2866 cm^{-1}, C=O stretching at 1723 cm^{-1}, C–O and C–C stretching at 1293 cm^{-1}, asymmetric C–O–C stretching at 1239 cm^{-1}, symmetric C–O–C stretching at 1165 cm^{-1}, and the N–H vibrations at 1576 cm^{-1}, and 1461 cm^{-1}. These characteristic peaks remained significantly unchanged, implying that immobilization of UOx did not destroy the structural integrity of PCL/PEI nanofibers. However, C=O stretch vibrations of peptide linkages produced by amide I protein are appeared at 1640 cm^{-1} after immobilization of UOx. These results indicated that the successful binding of UOx onto PCL/PEI nanofibers.

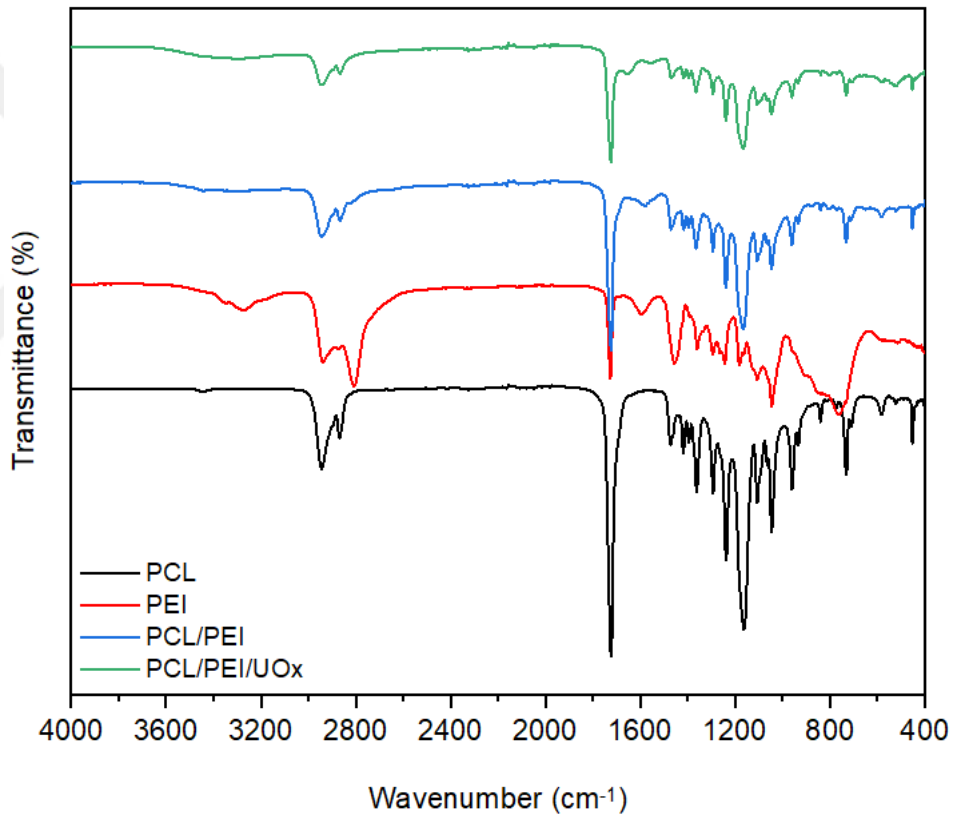

Figure 4.3 : FTIR spectra of pure PCL, PEI, pure PCL/PEI nanofibers and PCL/PEI/UOx nanofibers.

Moreover, the FTIR spectra of pure MB, PCL/PEI/MB nanofibers and PCL/PEI/MB/UOx nanofibers are shown in Figure 4.4. The FTIR spectrum of PCL/PEI/MB nanofibers showed the main characteristic bands of PCL/PEI and MB as aforementioned reported. The absorption bands at 3059, 2923 and 2846 cm^{-1} (CH_3 stretching vibrations of

dimethylamino groups), 1593 cm^{-1} (C=N and C=C vibrations), 1490 cm^{-1} (C–N vibrations), 1390 cm^{-1} (C=S+ stretching vibrations) and 1332 cm^{-1} (C–N stretching vibrations) are assigned to MB. By comparing with the spectrum of PCL/PEI/MB nanofibers, it was found that in PCL/PEI/MB/UOx nanofibers, higher absorption at 3367 cm^{-1} was observed because of immobilization of UOx. In addition, the typical vibration absorption peaks of N–H shifted to 1641 cm^{-1} from 1657 cm^{-1}. These changes confirmed that UOx was successfully immobilized on surfaces of PCL/PEI/MB nanofibers.

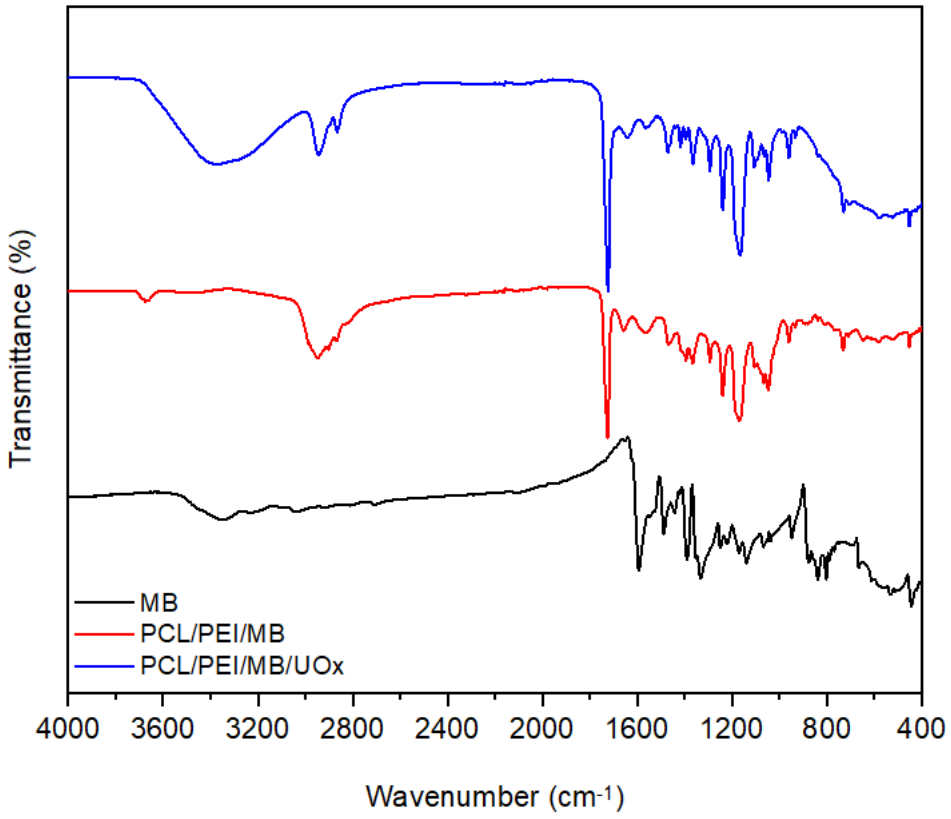

Figure 4.4 : FTIR spectra of pure MB, PCL/PEI/MB and PCL/PEI/MB/UOx nanofibers.

4.1.3. EDX analysis

The chemical composition of the PCL/PEI, and (B) PCL/PEI/UOx nanofibers was determined by EDX, as shown in Figure 4.5. The EDX pattern of PCL/PEI is mainly composed of only carbon (C), nitrogen (N) and oxygen (O) elements (Figure 4.5A). In addition, no new peaks related to other elements were detected after immobilization, however, the increased intensity of C and N content confirmed the successful

immobilization of UOx (Figure 4.5B). Moreover, the chemical composition of the PCL/PEI/MB, and PCL/PEI/MB/UOx nanofibers was further confirmed by EDX analysis (Figure 4.6). Figure 4.6A indicated the presence of elements C, N, O, sulfur (S) and chlorine (Cl) for EDX pattern of PCL/PEI/MB nanofibers. The presence of S, and Cl was due to using MB. Similarly, intensity of C, N and O content increased because of protein backbone after UOx immobilization (Figure 4.6.B). Therefore, it can be assumed that UOx was immobilized onto the surface of the PCL/PEI, and PCL/PEI/MB nanofibers.

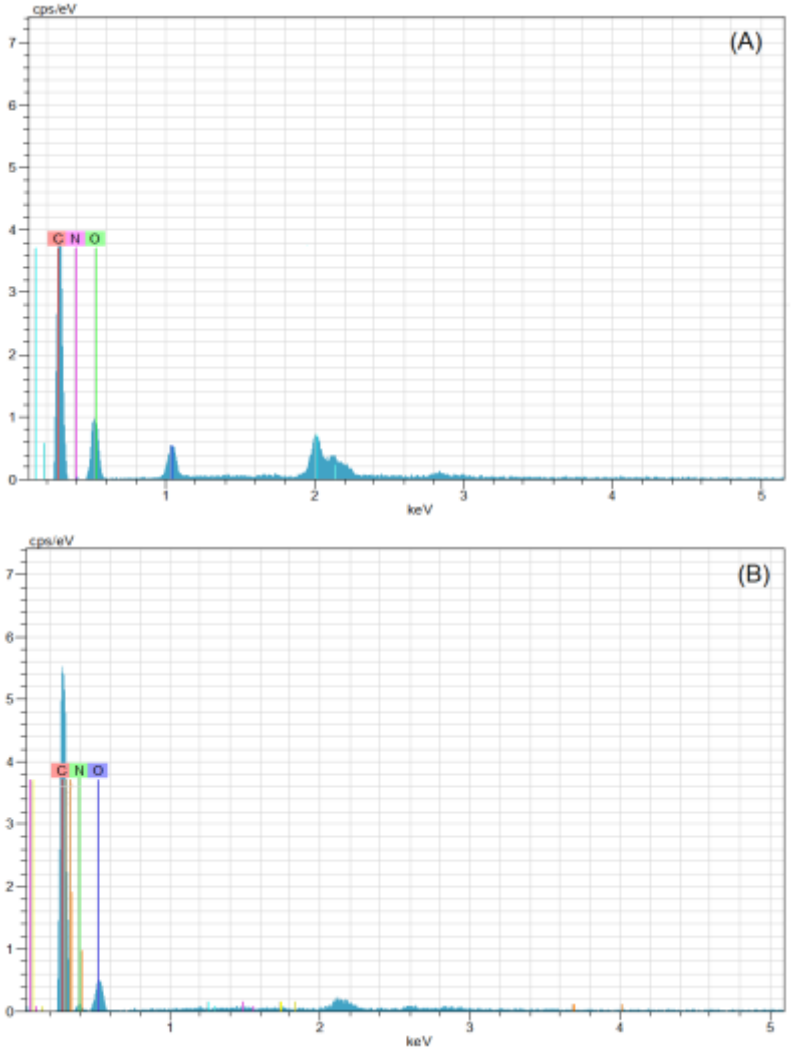

Figure 4.5 : EDX spectra of (A) PCL/PEI, and (B) PCL/PEI/UOx nanofibers.

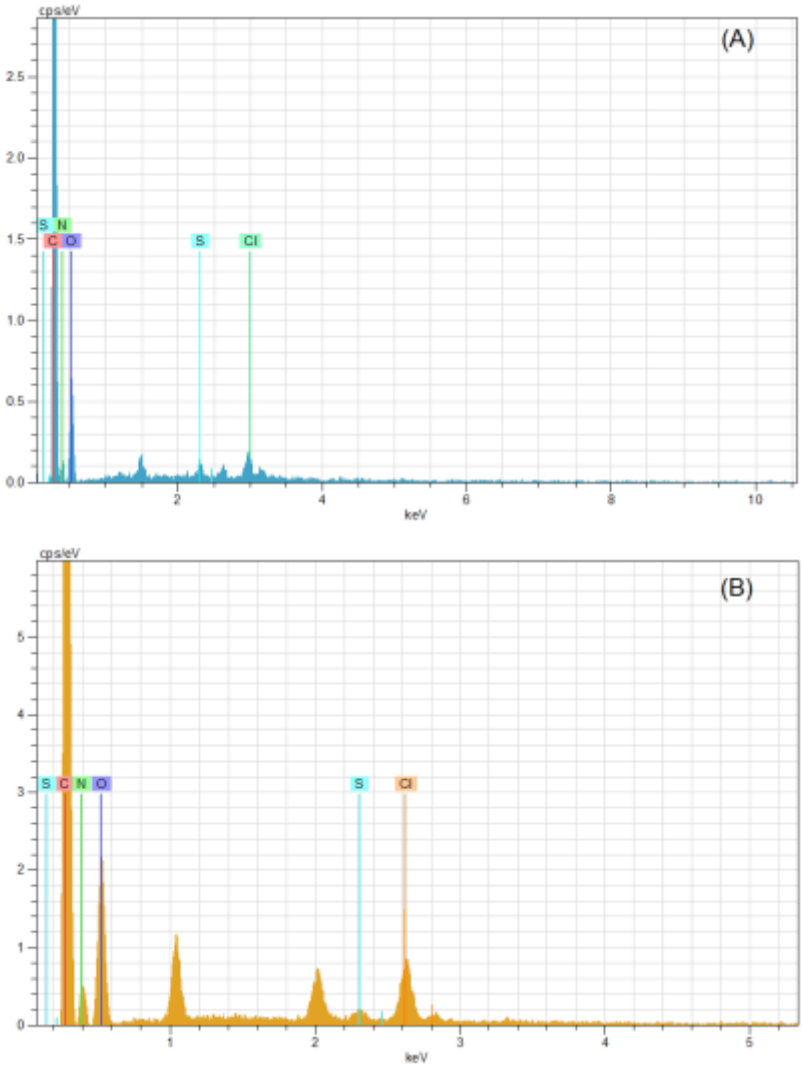

Figure 4.6 : EDX spectra of (A) PCL/PEI/MB, and (B) PCL/PEI/MB/UOx nanofibers.

4.1.4. XRD analysis

Figure 4.7 shows the XRD patterns of the PCL/PEI, PCL/PEI/UOx and PCL/PEI/MB/UOx nanofibers. The intensities of diffraction peaks at $2\theta = 21.52°$ and $2\theta = 23.86°$ assigned to the semi-crystalline structure of PCL/PEI. However, the immobilization of UOx led to a reduction in the intensity of all characteristic peaks that could result from the interaction of the PCL/PEI nanofibers with the enzyme, which is similar to that reported previously (Ates *et al*. 2018 and Monier *et al*. 2018).

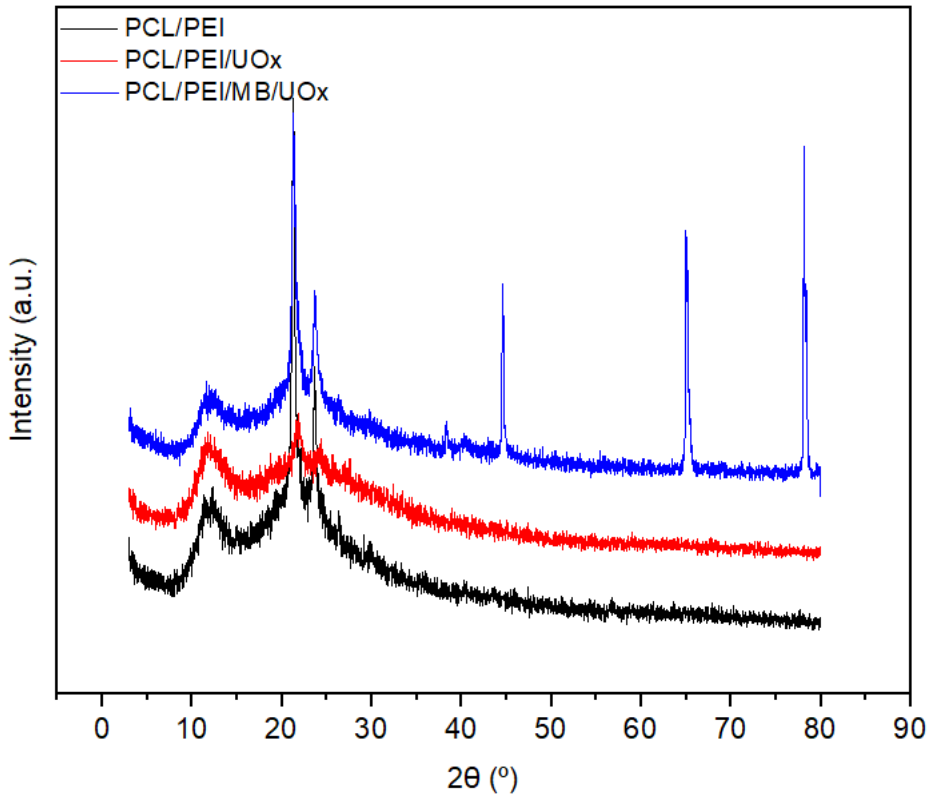

Figure 4.7 : XRD patterns of PCL/PEI, PCL/PEI/UOx and PCL/PEI/MB/UOx nanofibers.

4.1.5. Swelling ratio and water uptake

The equilibrium swelling ratio and water uptake results of the PCL, PCL/PEI and PCL/PEI/MB nanofibers are shown in Figure 4.8A. As expected, the addition of PEI increased the swelling ratio of the nanofibers from 41.7% to 322.8%. Because PEI is more hydrophilic than PCL, which is hydrophobic, blending these two polymers increased wettability. The swelling ratio (~763%) of PCL/PEI/MB nanofibers was higher than that of PCL/PEI nanofibers. This is because the presence of MB increases the spacing between the chains, which improves the penetration of water molecules into the nanofiber mesh, and as a result, the swelling rate increases. A similar scenario was observed for water uptake measurements. The water uptake abilities of the PCL, PCL/PEI and PCL/PEI/MB nanofibers are shown in Figure 4.8B. The nanofibers of PCL/PEI and PCL/PEI/MB absorbed water molecules up to ~75 and ~88%, respectively, which indicated addition of PEI and MB could improve water uptake behavior of nanofibers. Increased water uptake

of nanofibers could be due to hydrogen bonding among polymeric chains and water molecules (Le *et al*. 2022 and Mezhuev *et al*. 2021). The results obtained were confirmed by water contact angle measurements.

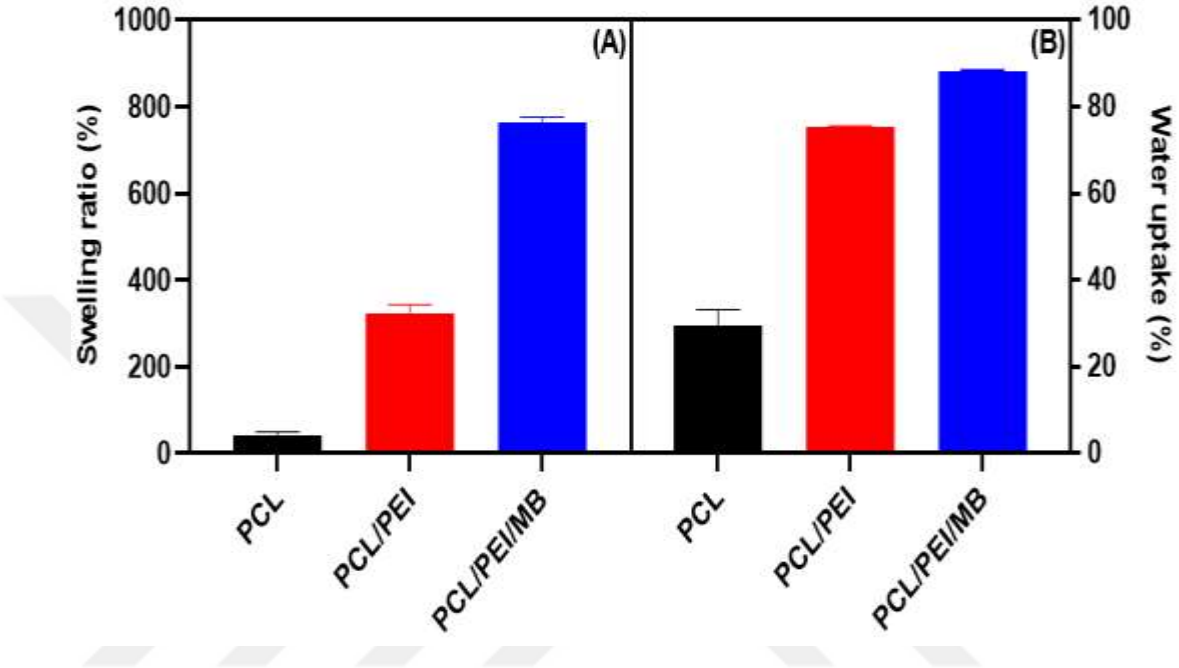

Figure 4.8 : Swelling ratio and water uptake of PCL, PCL/PEI and PCL/PEI/MB nanofibers.

4.1.6. Water contact angle (Wettability)

Wettability was determined by water contact angle measurement of the PCL, PCL/PEI and PCL/PEI/MB nanofibers. (Figure 4.9). As a result of PCL hydrophobicity, it exhibited contact angle 101.12 ±10.10^{o}. However, the water contact angle of the PCL/PEI nanofibers decreased to 38.68 ± 4.94◦, due to the hydrophilic nature of the PEI. Similarly, with the addition of MB to PCL/PEI nanofibers, the contact angle was greatly reduced to 19.07 ± 0.76◦. This result shows that the addition of MB leads to an increase in surface wettability for electrospin nanofibers.

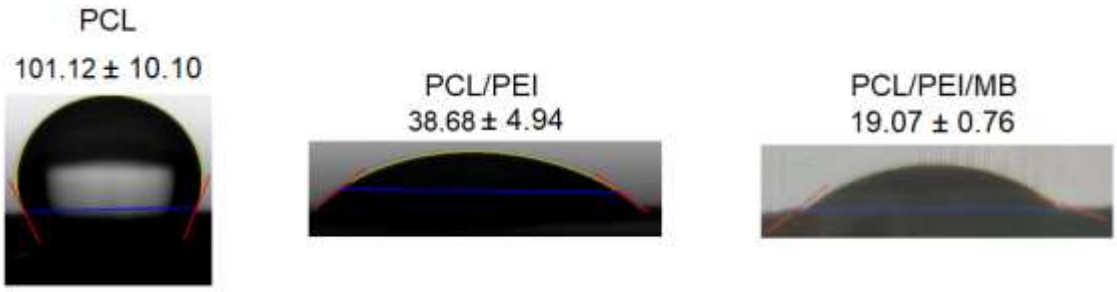

Figure 4.9 : Water contact angles of the PCL, PCL/PEI and PCL/PEI/MB nanofibers.

4.2.Enzyme Immobilization

4.2.1. Glutaraldehyde concentration

Glutaraldehyde as a crosslinking agent is generally used in intramolecular and intermolecular crosslinking reactions. However, excessive cross-linking can cause aggregation, precipitation, loss of activity and disruption of the internal dimensional structure of the enzyme structure. Therefore, optimization of glutaraldehyde concentration is an important parameter for enzyme immobilization. The effects of glutaraldehyde concentration on the activity of UOx were investigated at 0%–5% (Figure 4.10). As a result of the binding between the amine groups of PEI and UOx, the highest enzyme activity was obtained when the glutaraldehyde concentration reached 0.25%. A significant decrease in the activity of immobilized UOx above 0.25% glutaraldehyde was observed. This reduction is probably due to excess glutaraldehyde, which can cause unavoidable chemical modification and denaturation effects (Shui *et al*. 2020 and Arana – Pena *et al*. 2020).

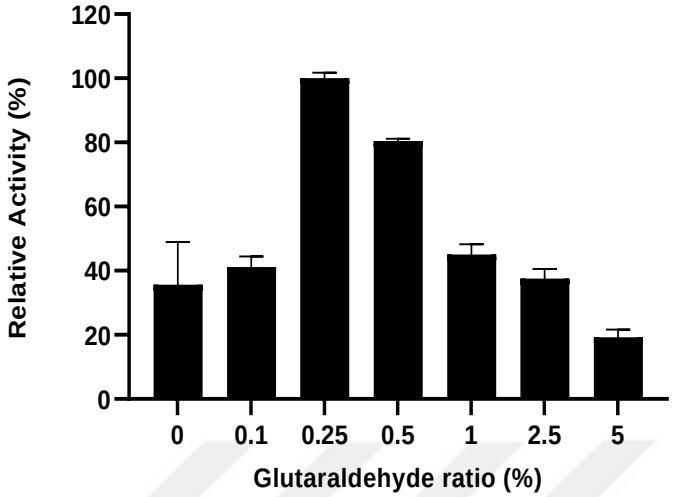

Figure 4.10 : The effect of glutaraldehyde ratio on the immobilization of UOx.

4.2.2. Enzyme concentration

In immobilization studies, it is essential to find the necessary enzyme concentration to immobilize. Figure 4.11 shows the effect of enzyme concentration on immobilization of UOx. Maximum activity was attained at 4 U of UOx/mL. However, further increasing the UOx concentration above the optimum level led to an increase in diffusion limitation and steric hindrance, resulting in a decrease in enzymatic activity. Similar observations were reported by several authors (Santiago – Acros *et al*. 2021 and Zdarta *et al*. 2020).

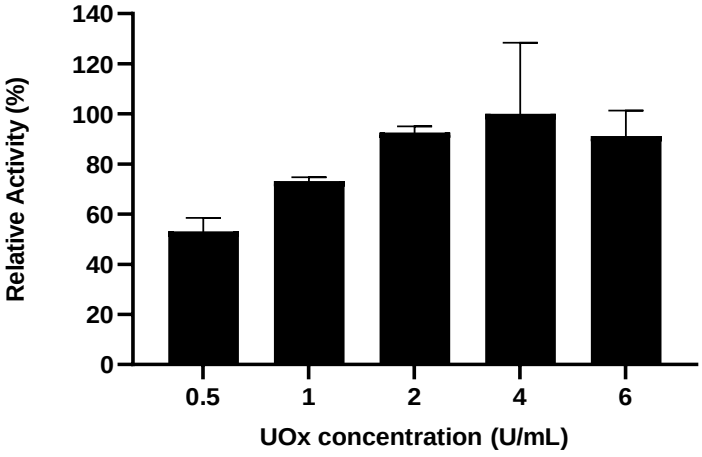

Figure 4.11 : The effect of UOx concentration on the immobilization of UOx.

4.3.Voltammetric Analysis

4.3.1. Cyclic Voltammetry (CV)

In the CV of 5 mM $K_3[Fe(CN)_6]$ of Bare QD SPCE (blue), PCL/PEI/ UOx/QD SPCE (green) and PCL/PEI/MB/UOx/QD SPCE (red) indicated that polymer and enzyme modification improved reliability as R^2 were elevated especially for anodes. In comparison the bare QD SPCE regression value was the lowest as R^2 was 0.9966 for cathode and 0.9707 for anode (Table 4.1 and Figure 4.12).

Table 4.1 : CV result of bare QD SPCE, PCL/PEI/UOx/QD SPCE and PCL/PEI/MB/UOx/QD SPCE

Electrode	**Cathode Equation**	**Cathode R^2**
Bare QD SPCE	Ipc = {(6.9852 ± 0.230244) $v^{1/2}$} + (2.00487 ± 1.0128)	(0.9970 ± 0.000644)
PCL/PEI/UOx/QD SPCE	Ipc = { (6.29673 ± 0.08162) ($v^{1/2}$) } + (4.4535 ± 0.52982)	(0.9987 ± 0.00024)
PCL/PEI/MB/UOx/QD SPCE	Ipc = {(4.7981 ± 0.05791) ($v^{1/2}$)} + (7.4987 ± 0.3979)	(0.9982 ± 0.00022)
Electrode	**Anode Equation**	**Anode R^2**
Bare QD SPCE	Ipa = {-(9.8624 ± 0.55617) ($v^{1/2}$)} + (14.032 ± 2.446)	(0.9760 ± 0.00367)
PCL/PEI/UOx/QD SPCE	Ipa = { (-6.1932 ± 0.06875) ($v^{1/2}$) } - (3.3385 ± 0.63507)	(0.99903±0.000244)
PCL/PEI/MB/UOx/QD SPCE	Ipa = {(-4.6926±0.04718) ($v^{1/2}$)} - (6.4812 ± 0.40844)	(0.9984± 0.000311)

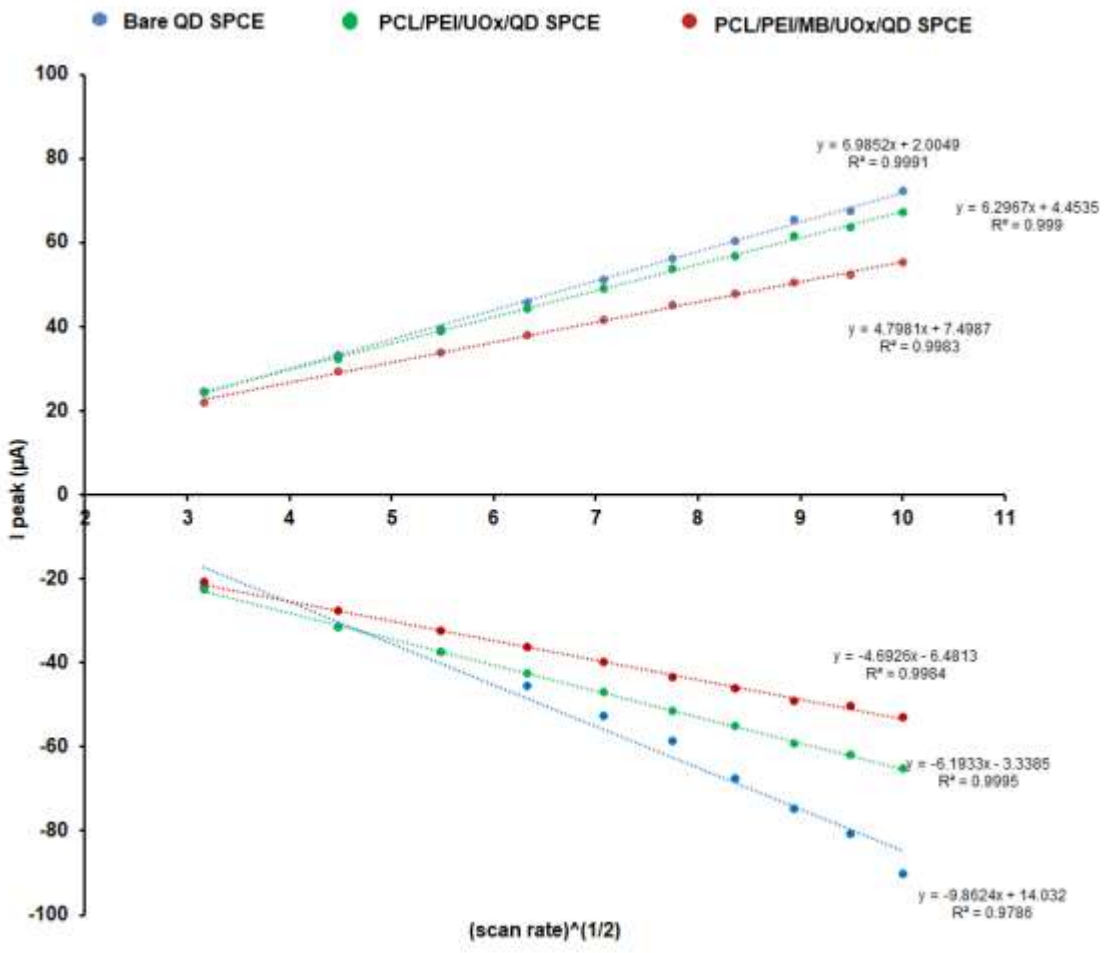

Figure 4.12 : CV graph of 5 mM $K_3[Fe(CN)_6]$ between bare QD SPCE (blue), PCL/PEI/UOx/QD SPCE (green) and PCL/PEI/MB/UOx/QD SPCE (red).

4.3.2. Ratio between peak anode and cathode (Ipa / Ipc)

As a result of CV in $K_3[Fe(CN)_6]$ of electrodes with ratio calculation of cathodic and anodic peak current (Ipc/Ipa), it was found that the PCL/PEI/MB/UOx/QD SPCE reached the highest Ipc/Ipa ratio as 1.04603 ± 0.00611. Meanwhile PCL/PEI/UOx/QD SPCE was the second as Ipc/Ipa 1.0417 ± 0.00807. In contrast bare QD SPCE was the lowest as 0.9591 ± 0.08553 (Figure 4.13 and 4.14).

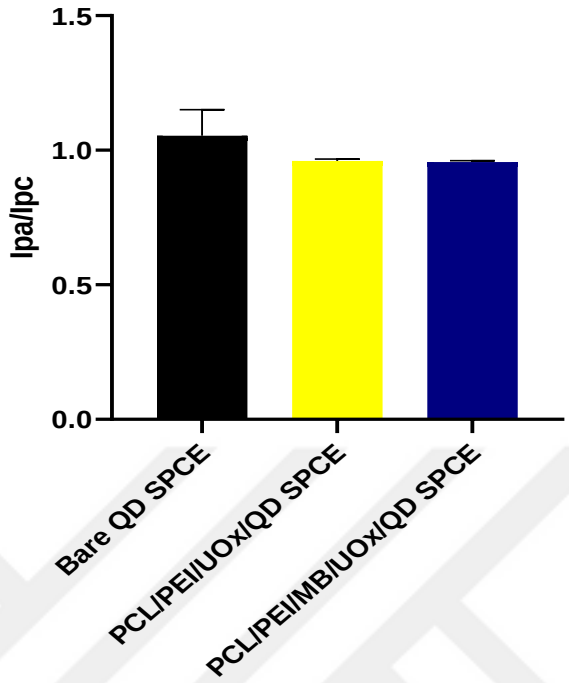

Figure 4.13 : Ratio between peak anode (Ipa) and peak cathode (Ipc) of electrodes in CV 5 mM $K_3[Fe(CN)_6]$.

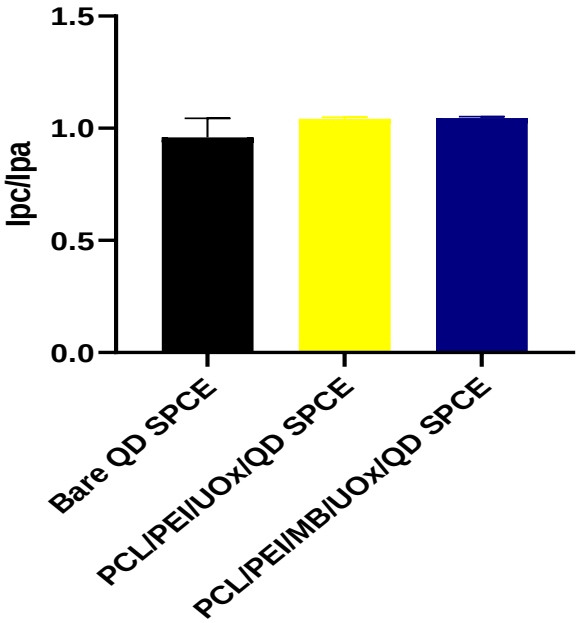

Figure 4.14 : Ratio between peak anode (Ipc) and peak cathode (Ipa) of electrodes in CV 5 mM $K_3[Fe(CN)_6]$.

4.3.3. Electroactive area of bare and modified QD SPCE

Apart from this the depletion of electroactive area was occurred on both of modified electrodes in which the PCL/PEI/MB/UOx/QD SPCE was the lowest by (1.5774 ± 0.1704) cm^2. Also PCL/PEI/UOx/QD SPCE was lower as (1.8504 ± 0.017903) cm^2 than its highest bare QD SPCE counterpart (2.0226 ± 0.03804) cm^2 (Figure 4.15).

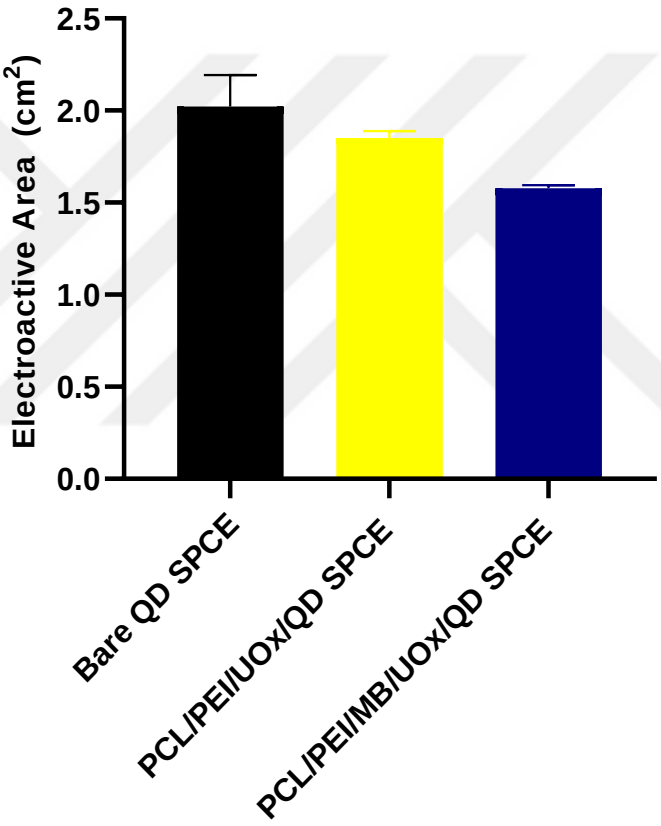

Figure 4.15 : Electroactive areas of bare QD SPCE, PCL/PEI/UOx/QD SPCE and PCL/PEI/MB/UOx/QD SPCE.

4.3.4. DPV measurements

DPV measurements were carried out for PCL/PEI/UOx/QD SPCE (non MB) and PCL/PEI/MB-UOx-QD SPCE (MB modified) with UA concentration between 5 and 52 µM (Figure 4.16). It was obtained that modification with polymer and enzyme improves reliability as both group exhibited regression value (R^2) greater than 0.99. Notably the

methylene blue (MB) modified and unmodified non MB R^2 was 0.9988 and 0.9947 respectively (Table 4.2 and Figure 4.17).

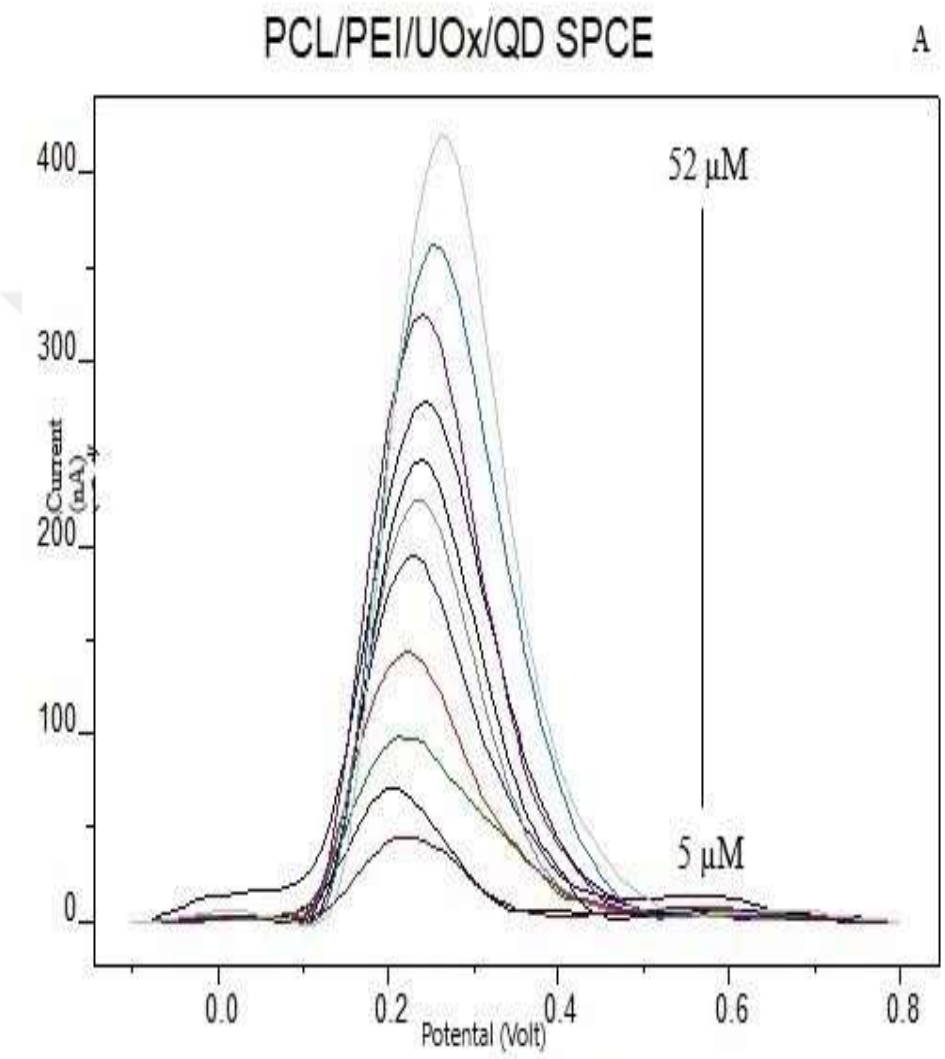

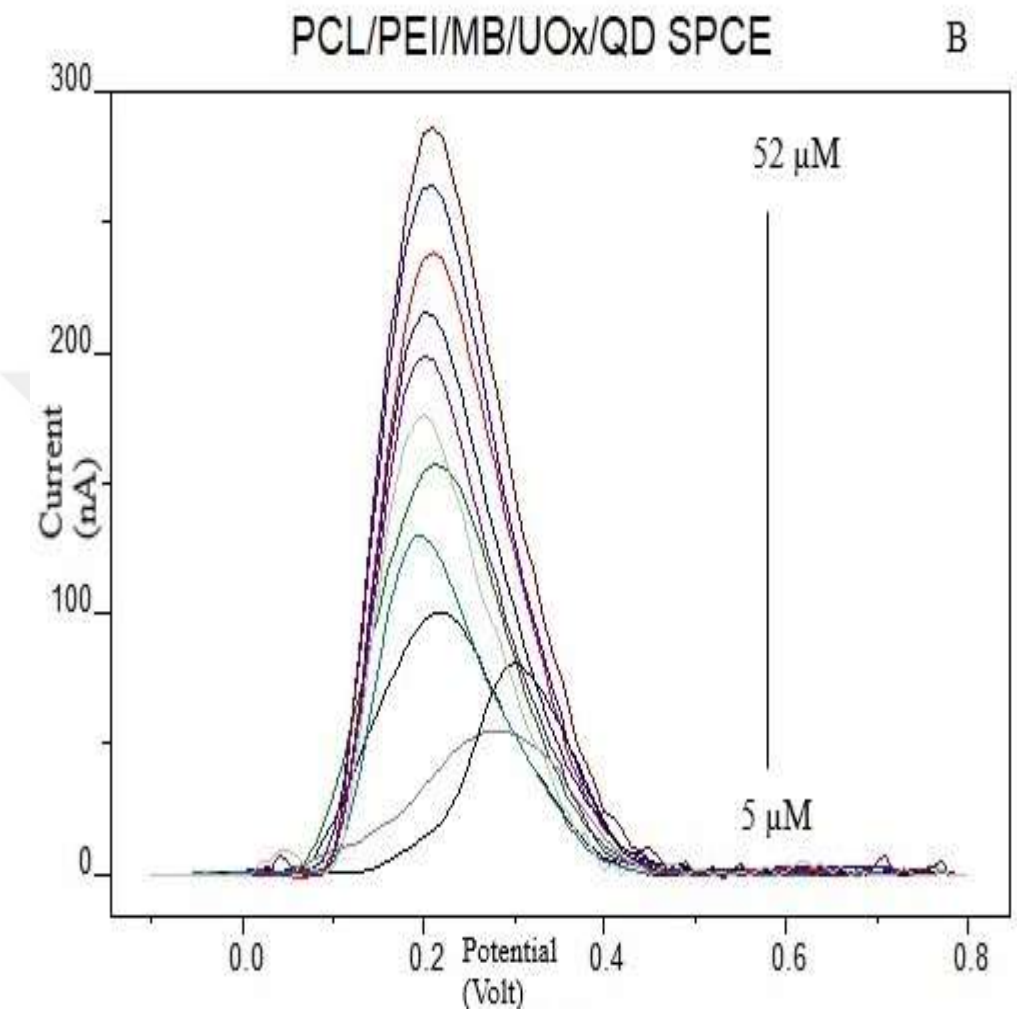

Figure 4.16 : DPV peaks of three minutes enzymatic reaction (a) PCL/PEI/UOx/QD SPCE and (b) PCL/PEI/ MB/UOx/QD SPCE.

Table 4.2 : Regression equation of DPV and LoD of PCL/PEI/UOx/QD SPCE and PCL/PEI/ MB/UOx/QD SPCE.

Electrode	Regression Equation	R^2	LoD (µM)
PCL/PEI/UOx/QD SPCE	Ip = {(0.0078 ± 0.000067)[UA]} - (0.0075 ± 0.00131)	0.9947	3.9619 ± 0.588
PCL/PEI/MB/UOx/QD SPCE	Ip = {(0.005 ± 0.000067)[UA]} + (0.0262 ± 0.0068)	0.9988	1.8598± 0.2345

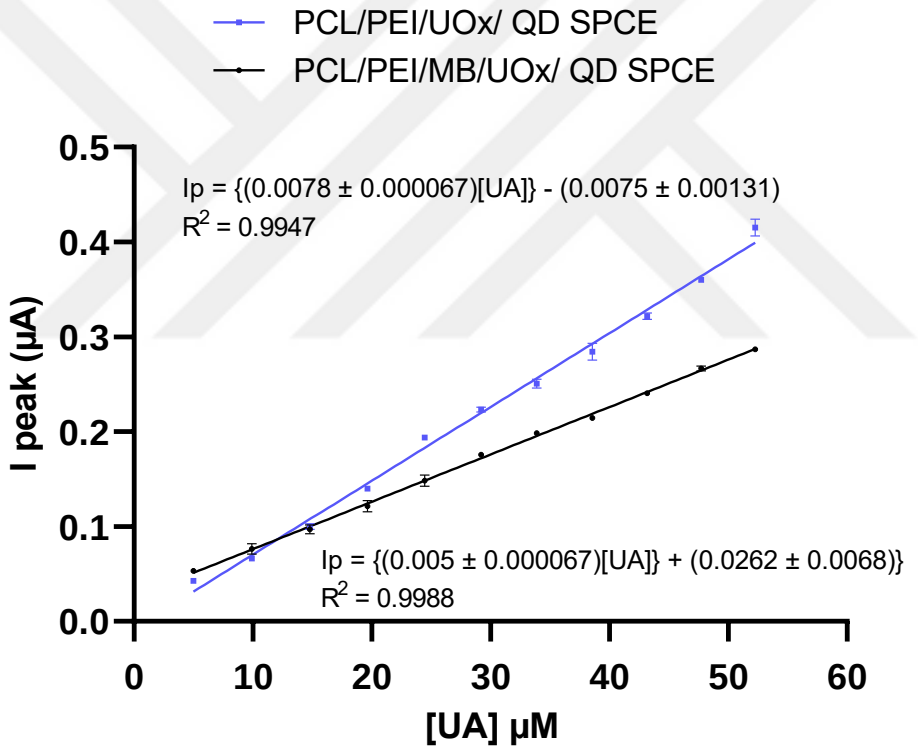

Figure 4.17 : DPV result of PCL/PEI/UOx/QD SPCE and PCL/PEI/ MB/UOx/QD SPCE.

Sensitivity value is obtained in accordance to the slope of DPV calibration curve of each modified electrodes. The value was 0.0078 ± 0.000067 and 0.005 ± 0.000067 µA μM^{-1} for PCL/PEI/UOx QD SPCE and PCL/PEI/MB/UOx/QD SPCE respectively (Table 4.3).

Table 4.3 : Sensitivity of PCL/PEI/UOx/QD SPCE, and PCL/PEI/MB/UOx/QD SPCE.

Electrode	Sensitivity ($\mu A\ \mu M^{-1}$)
PCL/PEI/UOx/QD SPCE	0.0078 ± 0.000067
PCL/PEI/MB/UOx/QD SPCE	0.005 ± 0.000067

4.3.4. UOx kinetic parameters from DPV

Owing to Lineweaver – Burk fitting, both electrode showed the linear correlation between 1/[C] and 1/Ipeak. Meanwhile the Km values of PCL/PEI/UOx/QD SPCE, and PCL/PEI/MB/UOx/QD SPCE were 212.6354 ± 49.6824, and 34.8489 ± 1.10132 μM, respectively (Table 4.4 and Figure 4.18).

Table 4.4 : KmApp values of PCL/PEI/UOx/QD SPCE, and PCL/PEI/MB/UOx/QD SPCE.

Electrode	KmApp (μM)	R^2
PCL/PEI/UOx/QD SPCE	212.6354 ± 49.6824	0.9996
PCL/PEI/MB/UOx/QD SPCE	34.8489 ± 1.10132	0.9961

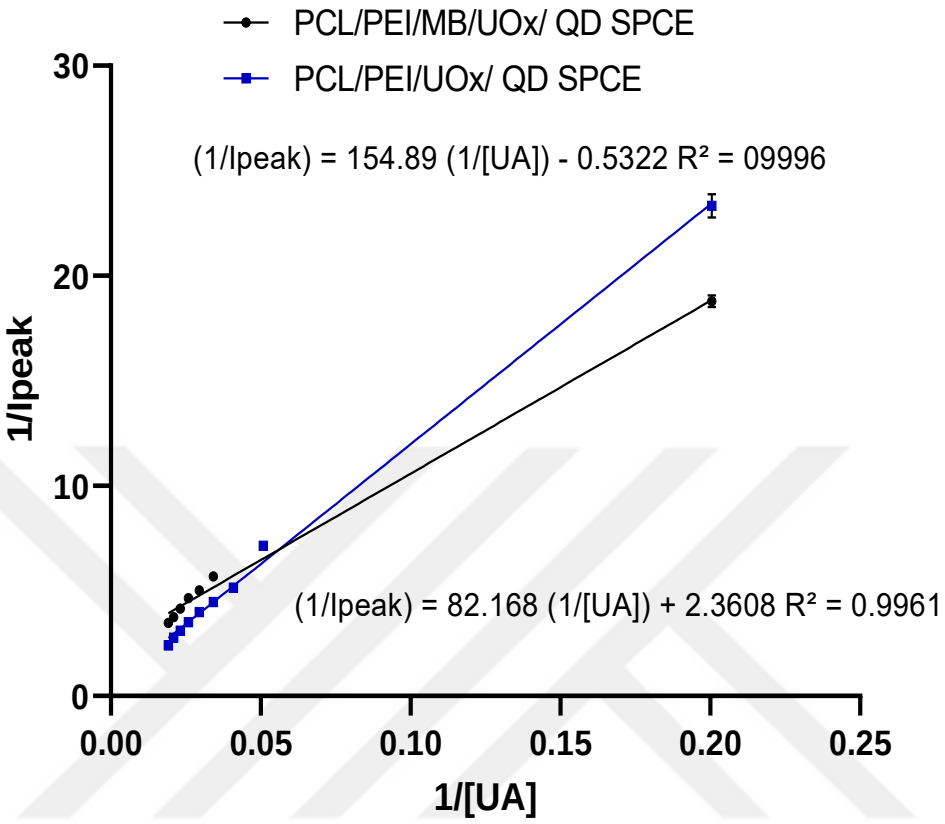

Figure 4.18 : Lineweaver-Burk plots of UOx enzyme in PCL/PEI/MB/UOx/QD SPCE and PCL/PEI/UOx/QD SPCE.

4.3.5. Storage stability

The result of stability test indicated the steady decrease of peak within four weeks in both electrodes (Figure 4.19). In addition, the MB modified electrode dropped from (99.0723 ± 0.3544) % to (92.4272 ± 2.3622) % remaining current. In contrast non MB electrode decreased from (97.2503 ± 1.1037) to (87.6289 ± 3.5407) %

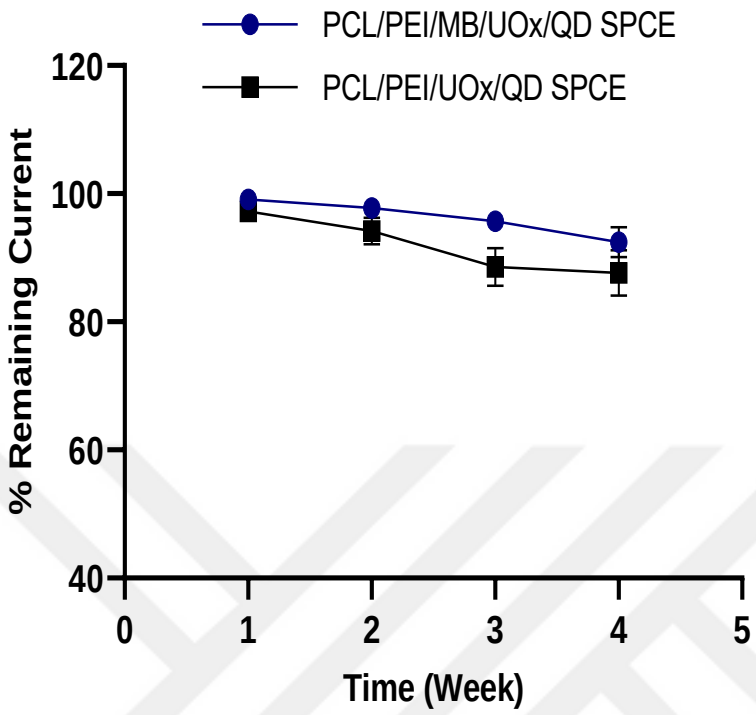

Figure 4.19 : Stability test of PCL/PEI/UOx/QD SPCE (black), and PCL/PEI/MB/UOx/QD SPCE (blue).

4.3.6. EIS measurements

EIS measurements were carried out in 5 mM $K_3[Fe(CN)_6]$ for bare QD SPCE (black dot line), PCL-PEI/MB/UOx/QD SPCE (green dot line) and PCL-PEI/UOx/QD SPCE (red dot line). Bare QD SPCE did not exhibit any semicircle while PCL/PEI/UOx/QD SPCE ($5.3381 \times 10^4 \pm 4.2444$ Ω) exhibited broader semicircle than PCL/PEI/MB/UOx/QD SPCE ($1.8768 \times 10^4 \pm 1.7778$ Ω).

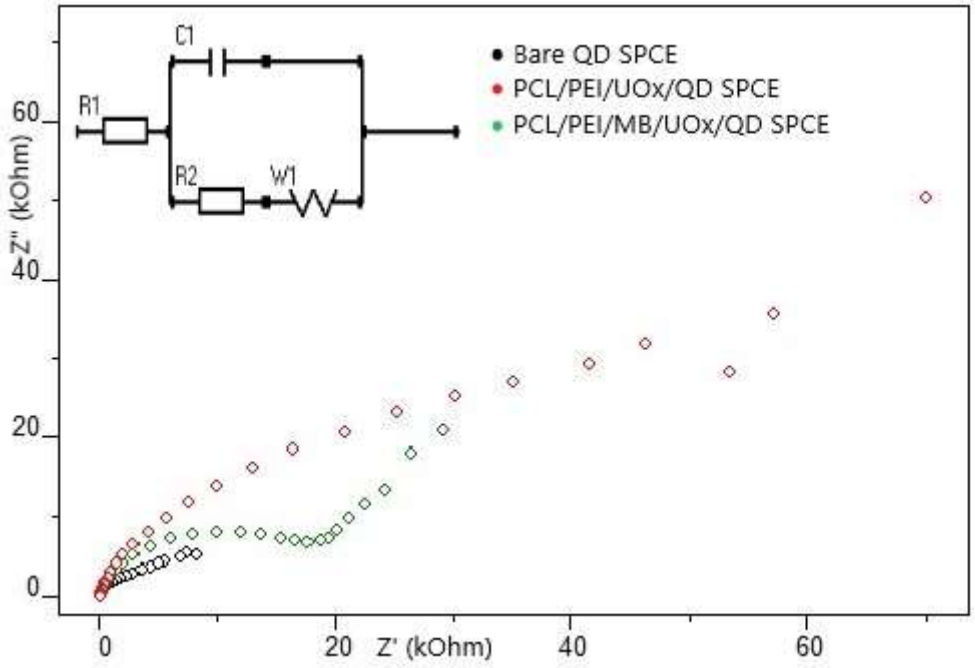

Figure 4.20 : EIS curves of for bare QD SPCE (black dot line), PCL-PEI/MB/UOx/QD SPCE (green dot line), and PCL-PEI/UOx/QD SPCE (red dot line) in 5 mM $K_3[Fe(CN)_6]$.

4. Interference Test

Interference test was conducted by DPV of UA (30 μM) within mixed interference which consisted of glucose (1 mM), Lactic Acid (0.25 mM), Ascorbic Acid (0.25 mM), dopamine (10 μM) and urea (0.25 mM). It was obtained that the remaining current was 95.00945 % for MB UOx and 82.063 % for non MB UOx respectively (Figure 4.21).

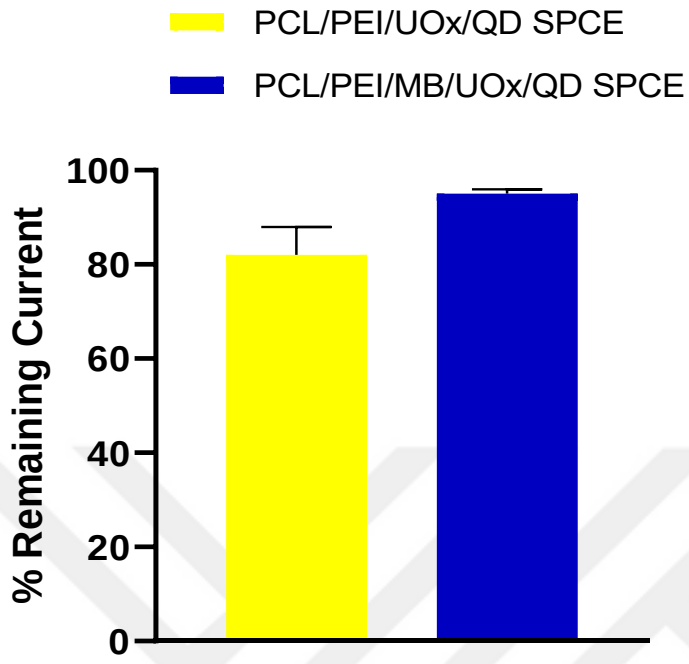

Figure 4.21 : Percentage of remained peak current after interference test.

5. DISCUSSION

Electrospinning stability and homogeneity is exhibited by both PCL/PEI/ UOx and PCL/PEI/ MB/UOx nanofiber in result of SEM as the fiber is beadles and Taylor cone appeared (van de Voorde *et al*.2022). In correlation to solvent mixture, homogeneity is correlated to solvent as it influences conductivity and electrospinnability which subsequently emerging the nanofibrous interconnection (Asadian *et al*. 2019). In agreement of our result which diameter is 100 and 400 nm, diameter change which is found during SEM analysis, solvent system is influential as homogeneity formation is led by solubility. As a result of PCL high solubility in organic solvent, homogeneity is generated by the absence of beads and droplets in fiber. (Radisavljevic *et al*. 2018 and Garrudo *et al*. 2021). In this study, glutaraldehyde was used crosslinker for bounding of UOx on the nanofiber membrane. All steps were characterized with FTIR, SEM, EDX and XRD.

Immobilized enzyme unit affects the activity in which certain unit will drive the highest or lowest activity. Owing to definition of activity, one unit is the amount of enzyme which capable to convert 1 μmol substrate in one minute at specific assay condition. In addition, immobilized activity is theoretical activity of bounded enzyme to the carrier while recovered activity is the real activity which catalyze the substrate after immobilization. Meanwhile recovered activity is strongly affected by the hydrophobicity of carrier. (Santiago – Arcos *et al*. 2021). Consequently, in this study, saturation was reached after maximum activity of 4 U/mL enzyme unit on the covered QD SPCE.

As a result of polymer covering of electrode surface, CV peak of polymer coated electrode was lower than its bare counterpart. In accordance to redox reaction between $[Fe(CN)_6]^{3-}$ and $[Fe(CN)_6]^{4-}$ ligand exchange is available. Reversibility in both modified electrode is showed as R^2 is greater than 0.99 and Ipa/Ipc is around 1. In contrast, the bare counterpart did not exhibit reversibility as R^2 anode is 0.975 and higher absorption of reduced species as Ipa/Ipc ratio 1.067 (Nagar *et al*. 2019, Kanso *et al*. 2017 and Frenzel *et al*. 2017). In addition, depletion of electroactive area in PCL/PEI UOx electrode took place because of coating and porosity of ionomer (Eguilaz *et al*. 2014).

Owing to DPV principle with Randles – Sevcik equation (25^{o}C), it is noted that peak current is proportional with concentration by the equation :

$$I_p = 2.69\ x\ 10^5 x(n^{3/2}) x A x C x (D_o)^{1/2} x v^{1/2}$$

Ip is anodic peak current, n for electron transfer number, A for electrode surface area, C for concentration, D for coefficient diffusion and v for scan rate. Meanwhile for CV, peak is proportional with square root of scan rate. Hence for DPV linear regression plot the correlation between I peak (Y) and Concentration (X) while for CV it plots $v^{1/2}$ (x) and I peak (y) (Lorenzetti *et al*. 2020). In both of CV and DPV, peak current of PCL/ PEI coated electrode was lower than its bare counterpart due to cationic polymer of PEI block the electrostatic interaction. Consequently, analyte diffusion of coated electrode is diminished (Kim *et al*. 2020 and Hernandez – Aldave *et al*. 2018).

Modification with MB improves the reliability as it reached R^2 0.9988 with LoD and sensitivity 1.8598 ± 0.2345 µM and 0.005 ± 0.000067 µA/µM. In contrast, without MB exhibited lower reliability as R^2 0.9947 with LoD and sensitivity 3.9619 ± 0.588 µM and 0.0078 ± 0.000067 µA/ µM. Hence, methylene blue addition improves sensitivity by facilitating electron transfer between hydrolyzed analyte and electrode surface. Subsequently, MB mediator also carries out redox after exposed to enzymatic product. Also, MB is pH sensitive redox reporter which shows redox potential alteration with solution pH. Thereafter, electrochemical signal as current is released (Wang *et al*. 2021, Gonzalez – Fernandez *et al*. 2022). Meanwhile, subsequent data processing of DPV utilized baseline subtracting to prevent error from shifting due to pH alteration (Marin *et al*. 2020 and Merlos Rodrigo *et al*. 2017).

$$\frac{1}{I} = \left[\frac{KmApp}{Imax}\left(\frac{1}{[UA]}\right)\right] + \frac{1}{Imax}$$

Inverse substrate and inverse current was plotted into x and y axis respectively to represent the Lineweaver – Burk result. Meanwhile Michaelis – Menten constant (Km) corresponds to the intercept to x axis (Aigner *et al*. 2017). The obtained K_M^{App} for PCL/PEI/UOx/QD SPCE and PCL/PEI/MB/UOx/QD SPCE was 212.6354 ± 49.6824 and 34.8489 ± 1.10132 µM respectively. In comparison to Quintero–Jaime *et al*. (2021), low Km value corresponds to high affinity between enzyme and substrate.

Table 5 : Comparison of performance with other UA enzymatic electrochemical biosensors

Electrode - Modifier	Method	Range (µM)	LoD (µM)	References
UOx/Chi – Gr/PB/ SPCE	FIA	2.5 - 400	2.5	Jirakunakorn *et al.* (2020)
CNT-CMC/Au/ UOx	CA	20 - 2700	2.8	Fukuda *et al*. 2020
UOx /CNT/Au/HRP/SPCE	CV	50 – 650	9.91	Bhusan *et al.* (2019)
GO/GCE/ UOx	Amperometric	20 – 490	3.45	Omar *et al*. 2016
UOx /SPCE-PB	CA	30 - 300	10	Piermarini *et al.* 2013
Au-rGO/ITO/ UOx	DPV	50 – 800	7.32	Verma *et al*. 2019
4-ASA/PB/GCE / UOx	Amperometry	10 – 200	3.0	Da Cruz *et al*. 2017
PVA–SbQ/SPCE/ UOx	CV	12 – 100	12	RoyChoudhury *et al*. 2018
MCM@41– UOx –TD-AgSA Transducer	Amperometry	50 - 800	18.5	Tvorynska *et al.* 2021
PCL/PEI/UOx/QD SPCE	DPV	4.97 - 52	3.9619	*This Work*
PCL/PEI/MB/ UOx /QD SPCE	DPV	4.97 - 52	1.895	*This Work*

After four week storage, DPV peak current was remained 99 to 92 % for PCL/PEI/MB/UOX/QD SPCE and 97 to 82 % for and PCL/PEI/UOx/QD SPCE respectively. In correlation to the stability principle, remaining current is indicator of electrode functionality after storage (Bocanegra – Rodriguez *et al*. 2021 and Marquitan *et al*. 2020). Moreover, 4 weeks is required as polymer modified electrode is influenced by layer thickness and enzyme loading capacity (Calitri *et al*. 2020). In correlation to the role of mediator particularly methylene blue (MB), faster electron transfer by methylene blue retains the remaining peak current which consequently lead the higher stability (Tahar *et al*. 2019 and Kuznowicz *et al*. 2021).

Apart from this EIS result exhibited semicircle resistance radius (Ret) from lowest to highest consecutively: Bare QD SPCE, PCL/PEI/MB/UOX/QD SPCE and PCL/PEI/UOx/QD SPCE. In comparison to Castano – Guerrero *et al*. (2021), binding of mediator decrease the charge transfer resistance which consequently dropped the semicircle diameter. Furthermore, it is regulated by redox properties of methylene blue as redox shuttle which is negatively charged. Subsequently structure is modified and resistance is dropped (Ortega *et al*. 2018). Meanwhile, 0.2 Volt was elected as starting potential as it was the peak potential of $K_3[Fe(CN)_6]$ during CV (Riedel *et al*. 2017). In addition, RC elements in ECM (Equivalent Circuit Model) of EIS was elected as easily transformed to time domain as temporal current – voltage behavior (Dierikx *et al*. 2020). Owing to resistance, EIS employs three resistance : C (Capacitance multi phase), R (charge transfer resistance) and W (Impedance for water vapor diffusion) which is displayed as semicircle by intercepting -Z' and Z" as imaginary component at low frequencies (Cruz – Manzo and Greenwood 2021).

In interference test reliability was still achieved by PCL/PEI/MB/UOX/QD SPCE and PCL/PEI/UOx/QD SPCE with DPV remaining current was 97.633 and 90.145 % respectively. The mixed interference test was carried out with simultaneous analysis of UOx 30 μM as analyte and involved mixture: ascorbic acid 0.25 mM, glucose 1 mM, Lactic acid 0.25 mM, dopamine 0.01 mM and urea 0.25 mM which aimed to resemble the blood serum chemical composition (Wang *et al*. 2021). Owing to the peak, ascorbic acid was located between potential 0.0 and 0.1 Volt while UA is between 0.1 and 0.2 Volt (Alba *et al*. 2022).

As a result of, in this research, it was concluded that modification of QD SPCE by using PCL/PEI nanofiber membrane with UOx immobilization improved its reliability. Firstly, reliability was reflected by the reversibility in Ipa/Ipc ratio of CV. Secondly, DPV of UOx immobilized coated electrode improved reliability by limit of detection 1.85 and 3.96 μM for PCL/PEI/MB/UOX/QD SPCE and PCL/PEI/UOx/QD SPCE, respectively. In addition, MB modified exhibited higher stability as the remaining current was 92 % after 4^{th} week storage as well as 95 % remaining current was detected after exposure to the mixed interference.

REFERENCES

Aigner M, Preissegger P, Kalcher K, Mehmeti E, Macheroux P, Edmondson D, Ortner A. 2017. Biosensor for the characterization of hMAO B inhibitors and the quantification of selegiline. *Talanta* 174 : 696 – 702 ; http://dx.doi.org/10.1016/j.talanta.2017.06.079

Alba AF, Totoricaguena – Gorrino J, Sanchez – Ilarduya MB, Ruiz – Rubio L, Vilas – Vilela JL, Lanceros – Mendez S, del Campo FJ. 2022. Laser – activated screen – printed carbon electrodes for enhanced dopamine determination in the presence of ascorbic and uric acid. *Electrochimica Acta* 399 : 139374 ; https://doi.org/10.1016/j.electacta.2021.139374

Angel N, Li S, Yan F, Kong L. 2022. Recent advances in electrospinning of nanofibers from bio-based carbohydrate polymers and their applications. *Trends in Food Science and Technology* 120 : 308 – 324 ; https://doi.org/10.1016/j.tifs.2022.01.003

Antuna – Jimenez D, Gonzalez – Garcia MB, Hernandez – Santos D, Fanjul – Bolado P. 2020. Review : Screen – printed electrodes modified with metal nanoparticles for small molecule sensing. *Biosensors* 10 : 9 ; http://dx.doi.org/10.3390/bios10020009

Aoun SB. 2017. Nanostructure carbon electrode modified with N – doped graphene quantum dots – chitosan nanocomposite : a sensitive electrochemical dopamine sensor. *Royal Society Open Science* 4 : 17119 ; http://dx.doi.org/10.1098/rsos.171199

Arana – Pena S, Rios NS, Mendez – Sanchez C, Lokha Y, Goncalves LRB, Fernandez – Lafuente R. 2020. Use of polyethylene imine to produce immobilized lipase multilayers biocatalysts with very high volumetric activity using octyl – agarose beads : Avoiding enzyme release during multilayer production. *Enzyme and Microbial Technology* 137 : 109535 ; https://doi.org/10.1016/j.enzmictec.2020.109535

Argaman O, Zelas ZBB, Fishman A, Rytwo G, Radian A. 2021. Immobilization of aldehyde dehydrogenase on montmorillonite using polyethyleneimine as a stabilization and bridging agent. *Applied Clay Science* 212 : 106216 ; https://doi.org/10.1016/j.clay.2021.106216

Asadian M, Grande S, Onyschchenko I, Morent R, Declerq H, De Geyter N. 2019. A comparative study one pre- and post-production plasma treatments of PCL films and nanofibers for improved cell-material interactions. *Applied Surface Sciences* 481 : 1554 – 1565 ; https://doi.org/10.1016/j.apsusc.2019.03.224

Ates B, Ulu A, Koytepe S, Noma SAA, Kolat VS, Izgi T. 2018. Magnetic – propelled Fe_3O_4 – chitosan carriers enhance L – asparaginase catalytic activity : a promising strategy for enzyme immobilization. *RSC Advances* 8 : 36063 – 36075 ; https://doi.org/10.1039/C8RA06346J

Baker SR, Banerjee S, Bonin K, Guthold M. 2016. Determining the mechanical properties of poly-ε-caprolactone (PCL) nanofibers using AFM and a novel fiber anchoring technique. *Materials Science and Engineering* C 59 : 203 – 212 ; http://dx.doi.org/10.1016/j.msec.2015.09.102

Bhusan P, Umansankar Y, RoyChoudhury S, Hirt PA, MacQuhaec FE, Borda LJ, Lev – Tov HA, Kirsner RS, Bhansali S. 2019. Biosensor for monitoring uric acid in wound

and its proximity : A potential wound diagnostic tool. *Journal of Electrochemical Society* 166 (10) : B830 – B836 ; https://doi.org/10.1149/2.1441910jes

Bigham A, Salehi AOM, Rafienia M, Salamat MR, Rahmati S, Rauci MG, Ambrosio L. 2021. Zn – substituted Mg_2SiO_4 nanoparticles – incorporated PCL – silk fibroin composite scaffold : A multifunctional platform towards bone tissue regeneration. *Materials Science and Engineering C* 127 : 112242 ; https://doi.org/10.1016/j.msec.2021.112242

Bocanegra – Rodriguez S, Molins – Legua C, Campins – Falco P, Giroud F, Gross AJ, Cosnier S. 2021. Monofunctional pyrenes at carbon nanotube electrodes for direct electron transfer H_2O_2 reduction with HRP and HRP – bacterial nanocellulose. *Biosensors and Bioelectronics* 187 : 113304 ; https://doi.org/10.1016/j.bios.2021.113304

Bollela P, Gorton L, Antiochia R. 2018. Review : Direct electron transfer of dehydrogenases for development of 3rd generation biosensors and enzymatic fuel cells. *Sensors* 18 : 1319 ; https://doi.org/10.3390/s18051319

Calitri G, Bollela P, Ciogli L, Tortolini C, Mazzei F, Antiochia R, Favero R. 2020. Evaluation of different storage processes of passion fruit (*Passiflora edulis* Sims) using a new dual biosensor platform based on a conducting polymer. *Microchemical Journal* 154 : 104573 ; https://doi.org/10.1016/j.microc.2019.104573

Castano – Guerrero Y, Moreira FTC, Sousa – Castillo A, Correa – Duarte MA, Sales MGF. 2021. SERS and electrochemical impedance spectroscopy immunoassay for carcinoembryonic antigen. *Electrochimica Acta* 366 : 137377 ; https://doi.org/10.1016/j.electacta.2020.137377

Cinti S, Mazzaraccchio V, Caccioti I, Moscone D, Arduini F. 2017. Carbon black – modified electrodes screen – printed onto paper towel , waxed paper and paraffin film ®. *Sensors* 17 : 2267 ; https://doi.org/10.3390/s17102267

Cruz – Manzo S, Greenwood P. 2021. Low frequency inductive loop in EIS measurements of an open – cathode polymer electrolyte fuel cell stack. Impedance of water vapor diffusion in the cathode catalyst layer. *J of Electroanalytical Chemistry* 900 : 115733 ; https://doi.org/10.1016/j.jelechem.2021.115733

da Cruz FS, de Sousa Paula F, Franco DL, dos Santos WTP, Ferreira LF. 2017. Electrochemical detection of uric acid using graphite screen – printed electrodes modified with Prussian Blue / poly (4 – aminosalicylic acid) / uricase. *J of Electroanalytical Chemistry* 806 : 172 – 179 ; https://doi.org/10.1016/j.jelechem.2017.10.070

Das P, Remigy J-C, Lahitte J-F, van der Meer AD, Garmy-Susini B, Coetsier C, Desclaux S, Bacchin P. 2020. Development of double porous poly-ε-caprolactone/chitosan polymer as tissue engineering scaffold. *Materials Science and Engineering* C 107 : 110257 ; https://doi.org/10.1016/j.msec.2019.110257

Decarpigny C, Bleta R, Ponchel A, Monflier E. 2021. Oxidation of 2,5-diformylfuran to 2,5-furandicarboxylic acid catalyzed by *Candida antarctica* Lipase B immobilized in cyclodextrin – templated mesoporous silica. The critical role of pore characteristics on

the catalytic performance. *Colloids and Surfaces B : Biointerfaces* 200 : 111606 ; https://doi.org/10.1016/j.colsurfb.2021.111606

Degorska O, Zdarta J, Synoradzki K, Zgola – Grzezkowiak A, Ciesielczyk F, Jesionowski T. 2021. From core – shell like structured zirconia / magnetite hybrid towards novel biocatalytic systems for tetracycline removal: Synthesis, enzyme immobilization, degradation and toxicity study. *J of Environmental Chemical Engineering* 9 : 105701 ; https://doi.org/10.1016/j.jece.2021.105701

Dierikx S, Weber A, Ivers – Tiffee E. 2020. How the distribution relaxation times enhances complex equivalent circuit models for fuel cells. *Electrochimica Acta* 355 : 136764 ; https://doi.org/10.1016/j.electacta.2020.136764

Dufay M, Jimenez M, Casetta M, Chai F, Blanchemain N, Stoclet G, Cazaux F, Bellayer S, Degoutin S. 2021. PCL covered PP meshes plasma – grafted by sulfonated monomer for the prevention of postoperative abdominal operations. *Materials Today Communications* 26 : 101968 ; https://doi.org/10.1016/j.mtcomm.2020.101968

Eguilaz M, Ferreyra NF, Rivas GA. 2014. Dispersions of hollow and bamboo – like multiwalled carbon nanotubes in polyethyleneimine : Critical analysis of the preparation conditions and applications for electrochemical sensing. *Electroanalysis* 26 : 2434 – 2444 ; https://doi.org/10.1002/elan.201400298

Frenzel N, Hartley J, Frisch G. 2017. Voltammetric and spectroscopic study of ferrocene and hexacyanoferate and the suitability of the redox couples as internal standards in ionic liquids. *Phys Chem Chem Phys* 19 : 28841 ; https://doi.org/10.1039/C7CP05483A

Fukuda T, Muguruma H, Iwasa H, Tanaka T, Hiratsuka A, Shimizu T, Tsuji K, Kishimoto T. 2020. Electrochemical determination of uric acid in urine and serum with uricase / carbon nanotube / carboxymethylcellulose electrode. *Analytical Biochemistry* 590 : 113533 ; https://doi.org/10.1016/j.ab.2019.113533

Galliani M, Tremolanti C, Signore G. 2019. Nanocarriers for protein delivery to cytosol : Assessing the endosomal escape of Poly(Lactide-co-Glycoside)-Poly(Ethylene Imine) nanoparticles. *Nanomaterials* 9 : 652 ; https://doi.org/10.3390/nano9040652

Gallops CE, Yu C, Ziebarth JD, Wang Y. 2019. Effect on protonation level and ionic strength on the structure of linear polyethyleneimine. *ACS Omega* 4 : 7255 – 7264 ; https://doi.org/10.1021/acsomega.9b00066

Garrudo FFF, Mikael PE, Rodrigues CAV, Udangawa RW, Paradiso P, Chapman CA, Hoffman P, Colaco R, Cabral JMS, Morgado J, Linhardt RJ, Ferreira FC. 2021. Polyaniline – polycaprolactone fibers for neural applications : Electroconductivity enhanced by pseudo – doping. *Materials Science and Engineering C* 120 : 111680 ; https://doi.org/10.1016/j.msec.2020.111680

Gil – Castell O, Ontoria – Oviedo I, Badia JD, Amaro – Prelezzo E, Sepulveda P, Ribes – Greus A. 2022. Conductive polycaprolactone / gelatin / polyaniline nanofibers as functional scaffolds for cardiac tissue regeneration. *Reactive and Functional Polymers* 170 : 105064 ; https://doi.org/10.1016/j.reactfunctpolym.2021.105064

Gomes FO, Maia LB, Delerue – Matos C, Moura I, Moura JJG, Morais S. 2019. Third – generation electrochemical biosensor based on nitric oxide reductase immobilized in multiwalled carbon nanotubes / 1 – n – butyl – 3 – methylimidazolium tetrafluoroborate nanocomposite for nitric oxide detection. *Sensors and Actuators B Chemical* 285 : 445 – 452 ; https://doi.org/10.1016/j.snb.2019.01.074

Gonzalez – Costas JM, Gomez – Fernandez S, Garcia J, Gonzalez – Romero E. 2020. Screen – printed electrodes – based technology : Environmental application to real time monitoring of phenolic degradation by phytoremediation with horseradish roots. *Science of the Total Environment* 744 : 140782 ; https://doi.org/10.1016/j.scitotenv.2020.140782

Gonzalez – Fernandez E, Staderini M, Marland JRK, Gray ME, Ucar A, Dunare C, Blair EO, Sullivan P, Tsiamis A, Greenhalgh SN, Gregson R, Clutton RE, Smith S, Terry JG, Argyle DJ, Walton AJ, Mount AR, Bradley M, Murray AF. 2022. In vivo application of an implantable tri – anchored methylene blue – based electrochemical pH sensor. *Biosensors and Bioelectronics* 197 : 113728 ; https://doi.org/10.1016/j.bios.2021.113728

Gonzalez – Sanchez MI, Gomez – Monedero B, Agrisuelas J, Iniesta J, Valero E. 2018. Highly activated screen – printed carbon electrodes by electrochemical treatment with hydrogen peroxide. *Electrochemistry Communications* 91 : 36 – 40 ; https://doi.org/10.1016/j.elecom.2018.05.002

Haider A, Haider S, Kang IK. 2018. A comprehensive review summarizing the effect of electrospinning parameters and potential application in nanofibers in biomedical and biotechnology. *Arabian J of Chemistry* 11 : 1165 – 1188 ; http://dx.doi.org/10.1016/j.arabjc.2015.11.015

Hernandez N, Iniesta J, Leguey VM, Armstrong R, Taylor SH, Madrid E, Rong Y, Castaing R, Malpass – Evans R, Carta M, McKeown NB, Marken F. 2017. Carbonization of polymers of intrinsic microporosity to microporous heterocarbon: Capactive pH measurements. *Applied Materials Today* 9 : 136 – 144 ; https://doi.org/10.1016/j.apmt.2017.06.003

Hernandez – Aldave S, Kaspar RB, Letterio MP, Tarat A, Yan Y, Bertoncello P. 2018. Quarternary phosphonium – based (TPQPCl) – ionomer / graphite nanoplatelets composites chemically modified electrodes : a novel platform for sensing applications. *J of Materials Chemistry C* 6 : 13293 – 13304 ; https://doi.org/10.1039/C8TC04967J

Hernandez – Ibanez N, Gomis – Berenguer A, Montiel V, Ania CO, Iniesta J. 2022. Fabrication of biocathode for formic acid production upon the immobilization of formate dehydrogenase from *Candida boidinii* on a nanoporous carbon. *Chemosphere* 291 : 133177 ; https://doi.org/10.1016/j.chemosphere.2021.133117

Hijazi A, Azambre B, Finqueneisel G, Vilbert F, Blin JL. 2019. High iodine adsorption by polyethyleneimine impregnated nanosilica sorbents. *Microporous and Mesoporous Materials* 288 : 109586 ; https://doi.org/10.1016/j.micromeso.2019.109586

Huang Y – J, Huang C – L, Lai R – Y, Zhuang C – H, Chiu W – H, Lee K – M. 2021. Microstructure and biological properties of electrospin in situ polymerization of

polycaprolactone – graft – polyacrylic acid nanofibers and its composite nanofiber dressings. *Polymers* 13 : 4246 ; https://doi.org/10.3390/polym13234246

Huo P, Han X, Zhang W, Zhang J, Kumar P, Liu B. 2021. Electrospin nanofibers of polycaprolactone / collagen as a sustained – release drug delivery system for artemisinin. *Pharmaceutics* 13 : 1228 ; https://doi.org/10.3390/pharmaceutics13081228

Hussain MH, Fook LP, Putri MKS, Tan HL, Bakar NFA, Radacsi N. 2021. Advances on ultra – sensitive electrospin nanostructured electrochemical and colorimetric sensors for diabetes mellitus detection. *Nano Materials Science* 3 : 321 – 343 ; https://doi.org/10.1016/j.nanoms.2021.05.001

Ji Y, Yang X, Ji Z, Zhu L, Ma N, Chen D, Jia X, Tang J, Cao Y. 2020. DFT – calculated IR spectrum amide I, II and III band contributions of N-methylacetamide fine components. *ACS Omega* 5 : 8572 – 8578 ; https://dx.doi.org/10.1021/acsomega.9b04421?ref=pdf

Jirakunakorn R, Khumngern S, Choosang J, Thavarungkul P, Kanatharana P, Numnuam A. 2020. Uric acid enzyme biosensor based on a screen – printed electrode coated with Prussian blue and modified with chitosan – graphene composite cryogel. *Microchemical Journal* 154 : 104624 ; https://doi.org/10.1016/j.microc.2020.104624

Kaczmarska K, Brycht M, Leniart A, Skrzypek S. 2017. Differential pulse voltammetric determination of an immunosuppressive drug teriflunomide on an edge plane pyrolytic graphite electrode. *RSC Advances* 7 : 26028 – 26036 ; https://doi.org/10.1039/C7RA00407A

Kanso H, Gonzalez – Garcia MB, Fernandez – Llano L, Ma S, Ludwig R, Fanjul – Bolado P, Hernandez – Santos D. 2017. Novel thin layer flow – cell screen – printed graphene electrode for enzymatic sensors. *Biosensors and Bioelectrodes* 93 : 298 – 304 ; http://dx.doi.org/10.1016/j.bios.2016.08.069

Kim JS, Lee S. 2019. Immobilization of trypsin from porcine pancreas onto chitosan nonwoven by covalent bonding. *Polymers* 11 : 1462 ; https://doi.org/10.3390/polym11091462

Kim MC, Kwak J, Lee SY. 2016. Sensing of uric acid via cascade catalysis of uricase and biomimetic catalyst. *Sensors and Actuators B* 232 : 744 – 749 ; http://dx.doi.org/10.1016/j.snb.2016.04.033

Kim S, Byeon CC, Kim SY. 2020. Electrochemical response of clay / polyelectrolyte composite barrier coatings. *Coatings* 10 : 1173 ; https://doi.org/10.3390/coatings10121173

Krampa FD, Aniweh Y, Awandare GA, Kanyong P. 2017. A disposable amperometric sensor based on high performance PEDOT : PSS/Ionic Liquid nanocomposite thin – film modified screen – printed electrode for the analysis of catechol in natural water samples. *Sensors* 17 (8) : 1716 ; https://doi.org/10.3390/s17081716

Kusmierek K, Swiatkowski A, Skrzypczynska K, Dabek L. 2021. Adsorptive and electrochemical properties of carbon nanotubes, activated carbon and graphene oxide

with relatively smaller surface area. *Materials* 144 : 496 ; https://www.mdpi.com/1996-1944/14/3/496#

Kuznowicz M, Jedrzak A, Leda A, Rebis T, Jesionowski T. 2021. Measurements of working parameters of external mediators for biodetectors based on polydopamine@magnetite nanoparticles. *Measurement* 184 : 109950 ; https://doi.org/10.1016/j.measurement.2021.109950

Le N – MN, Le – Vinh B, Friedl JD, Jalil A, Kali G, Bernkop – Schnurch A. 2022. Polyaminated pullulan a new biodegradable and cationic pullulan derivative for mucosal drug delivery. *Carbohydrate Polymers* 282 : 119143 ; https://doi.org/10.1016/j.carbpol.2022.119143

Lipinska W, Siuzdak K, Karczewski J, Dolega A, Grochowska K. 2021. Electrochemical glucose sensor based on the glucose oxidase entrapped in chitosan immobilized onto laser – processed Au – Ti electrode. *Sensors and Actuators B Chemical* 330 : 129409 ; https://doi.org/10.1016/j.snb.2020.129409

Liu J, Li G, Liu H, Zhou X. 1994. Purification and properties of uricase from *Candida* sp. and its application in uric acid analysis in serum. *Appl Biochem Biotechnol* 47 (1) : 57 – 63 ; https://doi.org/10.1007/bf02788675

Liu S, Bilal M, Rizwan K, Gul I, Rasheed T, Iqbal HMN. 2021. Smart chemistry of enzyme immobilization using various support of matrices – A review. *Int J of Biological Macromolecules* 190 : 396 – 408 ; https://doi.org/10.1016/j.ijbiomac.2021.09.006

Liu X, Wen M, Li J, Zhai F, Ruan J, Zhang L, Li S. 2011. High – yield expression, purification, characterization and structure determination of tag – free *Candida utilis* uricase. *Appl Microbiol Biotechnol* 92 : 529 – 537 ; https://doi.org/10.1007/s00253-011-3244-0

Lorenzetti AS, Sierra T, Domini CE, Lista AG, Crevilen AG, Escarpa A. 2020. Electrochemically reduced graphene oxide – based screen printed electrodes for total tetracycline determination by adsorptive transfer stripping differential pulse voltammetry. *Sensors* 20 : 76 ; https://doi.org/10.3390/s20010076

Madej M, Kochana J, Bas B. 2019. Determination of viloxazine by differential pulse voltammetry with boron – doped diamond electrode. *Monatshefte fuer Chemie* 150 : 1655 – 1665 ; https://doi.org/10.1007/s00706-019-2380-6

Marchetti M, Liuzzi A, Fermi B, Corsini R, Folli C, Speranzini V, Gandolfi F, Bettati S, Ronda L, Cendron L, Berni R, Zanotti G, Percudani R. 2016. Catalysis and structure of zebrafish urate oxidase provide insights into the origin of hyperuricemia in hominoids. *Scientific Reports* 6 : 38302 ; https://doi.org/10.1038/srep38302

Marin J, Serrano N, Arino C, Diaz – Cruz JM. 2020. A chemometric survey about the ability of voltammetry to discriminate pharmaceutical products from the evolution of signals as a function of pH. *Chemosensors* 8 (3) : 46 ; https://www.mdpi.com/2227-9040/8/3/46/htm#

Marquitan M, Ruff A, Bramini M, Herlitze S, Mark MD, Schuhmann W. 2020. Polymer / enzyme modified HF – etched carbon nanoelectrodes for single – cell analysis. *Bioelectrochemistry* 133 : 107487 ; https://doi.org/10.1016/j.bioelechem.2020.107487

Martin - Yerga D, Gonzalez – Garcia MB, Costa – Garcia A. 2014. Electrochemical immunosensor for anti – tissue transglutaminase antibodies based on the in situ detection of quantum dots. *Talanta* 130 : 598 – 602 ; http://dx.doi.org/10.1016/j.talanta.2014.07.010

Martin – Yerga D, Fanjul – Bolado P, Hernandez – Santos D, Costa – Garcia A. 2017. Enhanced detection of quantum dots by the magnetohydrodynamic effect for electrochemical biosensing. *Analyst* 142 : 1591 – 1600 ; https://doi.org/10.1039/C7AN00086C

Martinez – Reyes CP, Manjarrez – Reyna AN, Mendez – Garcia LA, Aguayo – Guerrero JA, Aguirre – Sierra B, Villalobos – Molina R, Lopez – Vidal Y, Bobadilla K, Escobedo G. 2020. Uric acid has direct proinflammatory effects on human macrophages by increasing proinflammatory mediators and bacterial phagocytosis probably by URAT1. *Biomolecules* 10 : 576 ; https://doi.org/10.3390/biom10040576

Mazzara F, Patella B, Aiello G, O'Riordan A, Torino C, Vilasi A, Inguanta R. 2022. Electrochemical detection of uric acid and ascorbic acid using r-GO/NPs based sensors. *Electrochimica Acta* 388 : 138652 ; https://doi.org/10.1016/j.electacta.2021.138652

Merlos Rodrigo MA, Molina – Lopez J, Jimenez Jimenez AM, Planells Del Pozo E, Adam P, Eckschlanger T, Zitka O, Richtera L, Adam V. 2017. The applıcation of curve fitting on the voltammograms of various isoforms of metallothioneins – metal complex. *Int J of Molecular Sciences* 18 (3) : 610 ; https://doi.org/10.3390/ijms18030610

Mezhuev YO, Vorobev IY, Plyuschchii IV, Krivoborodov EG, Arthyukov AA, Motyakin MV, Luss AL, Ionova IS, Kovarskii AL, Derevnin IA, Dyatlov VA, Alekperov RA, Toropygin IY, Volkov MA, Shtilman MI, Korshak YV. 2021. Chemical oxidative polymerization of methylene blue : Reaction mechanism and aspects of chain structure. *Polymers* 13 (13) : 2188 ; https://doi.org/10.3390/polym13132188

Mirceski V, Guziejewski D, Stoanov L, Gulaboski R. 2019. Differential Square – Wave voltammetry. *Anal Chem* 91 : 14904 – 14910 ; https://doi.org/10.1021/acs.analchem.9b03035

Mirzaei Z, Kordestani SS, Kuth S, Schubert DW, Detsch R, Roether JA, Blunk T, Boccaccini AR. 2020. Preparation and characterization of electrospun blend fibrous polyethylene oxide : polycaprolactone scaffolds to promote cartilage regeneration. *Advance Engineering Materials* 22 : 2000131 ; https://doi.org/10.1002/adem.202000131

Mirzaeinia S, Pazhang M, Imani M, Chaparzadeh N, Amani – Ghadim AR. 2020. Improving the stability of uricase from *Aspergillus flavus* by osmolytes : Use of response surface methodology for optimization of the enzyme stability. *Process Biochemistry* 94 : 86 – 98 ; https://doi.org/10.1016/j.procbio.2020.04.020

Miyazaki CM, Mishra R, Kinahan DJ, Ferreira M, Ducree J. 2017. Polyethylene imine / graphene oxide layer – by – layer surface functionalization for significantly improved

limit of detection and binding kinetics of immunoassays acrylate surfaces. *Colloids and Surfaces B : Biointerfaces* 158 : 167 – 174 ; http://dx.doi.org/10.1016/j.colsurfb.2017.06.042

Monier M, Shafik AL, El – Mekabaty A. 2019. Designing and investigation of photo – active gellan gum for the efficient immobilization of catalase by entrapment. *Int J of Biological Macromolecules* 161 : 539 – 549 ; https://doi.org/10.1016/j.ijbiomac.2020.06.079

Monteiro T, Almeida MG. 2019. Electrochemical enzyme biosensor revisited : Old solutions for new problems. *Critical Reviews in Analytical Chemistry* , 49 (1) : 44 – 66 ; https://doi.org/10.1080/10408347.2018.1461552

Musameh MM, Dunn CJ, Uddin MH, Sutherland TD, Rapson TD. 2018. Silk provides a new avenue for third generation biosensors : Sensitive, selective and stable electrochemical detection of nitric oxide. *Biosensors and Bioelectronics* 103 : 26 – 31 ; https://doi.org/10.1016/j.bios.2017.12.019

Nagar B, Balsells M, de la Escoura – Muniz A, Gomez – Romero P. 2019. Fully printed one – step biosensing device using graphene/AuNP composite. *Biosensors and Bioelectronics* 129 : 238 – 244 ; https://doi.org/10.1016/j.bios.2018.09.073

Nguyen HH, Lee SH, Lee UJ, Fermin CD, Kim M. 2019. Review : Immobilized enzymes in biosensor applications. *Materials* 12 : 121 ; http://dx.doi.org/10.3390/ma12010121

Nguyen TN, Rangel A, Migonney V. 2022. Correlating the degradation of functionalized polycaprolactone fibers and fibronectin adsorption using atomic force microscopy. *Polymer Degradation and Stability* 195 : 109788 ; https://doi.org/10.1016/j.polymdegradstab.2021.109788

Nicholas P, Pittson R, Hart JP. 2018. Development of simple, low cost chronoamperometric assay for fructose based on a commercial graphite – nanoparticle modified screen – printed carbon electrode. *Food Chemistry* 241 : 122 – 126 ; http://dx.doi.org/10.1016/j.foodchem.2017.08.077

Omar MN, Salleh AB, Lim HN, Tajudin AA. 2016. Electrochemical detection of uric acid via uricase – immobilized graphene oxide. *Analytical Biochemistry* 509 : 135 – 141 ; http://dx.doi.org/10.1016/j.ab.2016.06.030

Ortega PFR, de Paula PGF, de Castro MCM, Binatti I, Gonzalez Z, Blanco C, Santamaria R, Lavall RL. 2018. Mechanism and stability of a redox supercapacitor based on methylene blue : Effects of degradation of redox shuttle. *ACS Appl. Energy Materials* 1 : 2306 – 2316 ; http://dx.doi.org/10.1021/acsaem.8b00384

Piermarini S, Migliorelli D, Volpe G, Massoud R, Pierantozzi A, Cortese C, Palleschi G. 2013. Uricase biosensor based on a screen – printed electrode modified with Prussian blue for detection of uric acid in human blood serum. *Sensors and Actuators B* 179 : 170 – 174 ; https://doi.org/10.1016/j.snb.2012.10.090

Quintero – Jaime AF, Conzuelo F, Cazorla – Amoros D, Morallon E. 2021. Pyrroloquinilone quinone – dependent glucose dehydrogenase bioelectrodes based on one – step electrochemical entrapment over single – wall carbon nanotubes. *Talanta* 232 : 122386 ; https://doi.org/10.1016/j.talanta.2021.122386

Radisavljevic A, Stojanovic DB, Perisic S, Djokic V, Radojevic V, Rajilic – Stojanovic M, Uskokovic PS. 2018. Cefazolin – loaded polycaprolactone fibers produced via different electrospinning methods : Characterization, drug release and antibacterial effect. *European J of Pharmaceutical Sciences* 124 : 26 – 36 ; https://doi.org/10.1016/j.ejps.2018.08.023

Riedel M, Sabir N, Scheller FW, Parak WJ, Lisdat F. 2017. Connecting quantum dots with enzymes : mediator – based approaches for the light – directed read – out of glucose and fructose oxidation. *Nanoscale* 9 : 2814 - 2823 ; https://doi.org/10.1039/C7NR00091J

RoyChoudhury S, Umasankar Y, Hutcheson JD, Lev – Tov HA, Kirsner RS, Bhansali S. 2018. Uricase based enzymatic biosensor for non – invasive detection of uric acid by entrapment in PVA – SbQ polymer matrix. *Electroanalysis* 30 : 2374 – 2385 ; https://doi.org/10.1002/elan.201800360

Russo E, Drovandi S, Salvidio G, Verzola D, Esposito P, Garibotto G, Viazzi F. 2020. Increased serum uric acid levels are associated to renal arteriolopathy and predict poor outcome in IgA nephropathy. *Nutrition, Metabolism and Cardiovascular Diseases* 30 : 2343 – 2350 ; https://doi.org/10.1016/j.numecd.2020.07.038

Saito Y, Tanaka A, Node K, Kobayashi Y. 2021. Review : Uric acid and cardiovascular disease : A clinical review. *J of Cardiology* 78 : 51 – 57 ; https://doi.org/10.1016/j.jjcc.2020.12.013

Santiago – Arcos J, Velasco – Lozano S, Diamanti E, Cortajarena AL, Lopez – Gallego F. 2021. Immobilization screening and characterization of an alcohol dehydrogenase and its application to the multi – enzymatic selective oxidation of 1 – omega – diols. *Frontiers in Catalysis* 1 : 715075 ; https://doi.org/10.3389/fctls.2021.715075

Sharma D, Lee J, Seo J, Shin H. 2017. Development of a sensitive electrochemical enzymatic reaction based cholesterol biosensor using nanosized carbon interdigitated electrodes decorated with gold nanoparticles. *Sensors* 17 (9) : 2128 ; https://doi.org/10.3390/s17092128

Shui T, Adhikari BB, Chae M, Bressler DC. 2020. Evaluation of thermally hydrolyzed specific risk materials cross – linked with glutaraldehyde for tackifier applications. *Process in Organic Coatings* 140 : 105535 ; https://doi.org/10.1016/j.porgcoat.2019.105535

Suzuki N, Lee J, Loew N, Takashi – Inose Y, Okuda – Shimazaki J, Kojima K, Mori K, Tsugawa W, Sode K. 2020. Engineered glucose oxidase capable of quasi – direct electron transfer after a quick and easy modification with a mediator. *Int J of Molecular Sciences* 21 : 1137 ; https://doi.org/10.3390/ijms21031137

Szczesny J, Ruff A, Oliveira AR, Pita M, Pereira IAC, De Lacey AL, Schuhmann W. 2020. Electroenzymatic CO_2 fixation using redox polymer / enzyme – modified gas diffusion electrodes. *ACS Energy Letter* 5 : 321 – 327 ; https://doi.org/10.1021/acsenergylett.9b02436

Tahar AB, Szymczyk A, Tingry S, Vadgama P, Zelsmanne M, Tsujumura S, Cinquin P, Martin D, Zebda A. 2019. One year stability of glucose dehydrogenase confined in a

3D carbon nanotube electrode with coated poly – methylene green : Application as bioanode for a glucose biofuel cell. *Journal of Electroanalytical Chemistry* 847 : 113069 ; https://doi.org/10.1016/j.jelechem.2019.04.029

Topsoy OK, Muhammad F, Kolak S, Ulu A, Gungor O, Simsek M, Koytepe S, Ates B. 2022. Fabrication of electrospin polycaprolactone/chitosan nanofiber – modified screen – printed electrode for highly sensitive detection of diazinon in food analysis. *Measurement* 187 : 110250 ; https://doi.org/10.1016/j.measurement.2021.110250

Tvorynska S, Barek J, Josypcuk B. 2021. Flow amperometric uric acid biosensors based on different enzymatic mini – reactors : A comparative study of uricase immobilization. *Sensors and Actuators B. Chemical* 344 : 130252 ; https://doi.org/10.1016/j.snb.2021.130252

Van de Voorde B, Sensu B, De Vos L, Colenbier R, Baskan H, Geltmeyer J, Parmentier L, Van Daele L, Dmitriev RI, Pyl L, De Clerck K, Van Vlierberghe S. 2022. Electrospinning of Poly(decamethylene terephthalate) to support vascular graft applications. *European Polymer Journal* 165 : 111003 ; https://doi.org/10.1016/j.eurpolymj.2022.111003

Verma S, Choudhary J, Singh KP, Chandra P, Singh SP. 2019. Uricase grafted nanoconducting matrix based electrochemical biosensor for ultrafast uric acid detection in human serum samples. *Int J of Biological Macromolecules* 130 : 333 – 341 ; https://doi.org/10.1016/j.ijbiomac.2019.02.121

Voniatis C, Barczikai D, Gyulai G, Jedlovszky – Hadju A. 2021. Fabrication and characterization of electrospin polycaprolactone/polysuccinimide composite mashes. *J of Molecular Liquids* 323 : 115094 ; https://doi.org/10.1016/j.molliq.2020.115094

Wang F, Li R, Jian H, Huang Z, Wang Y, Guo Z, Gao R. 2020. Design and construction of an effective expression system with aldehyde tag for site – specific enzyme immobilization. *Catalysts* 10 (4) : 410 ; https://doi.org/10.3390/catal10040410

Wang Q, Liu Y, Campillo – Brocal JC, Jimenez – Quero A, Crespo GA, Cuartero M. 2021. Electrochemical biosensor for glycine detection in biological fluids. *Biosensors and Bioelectronics* 182 : 113154 ; https://doi.org/10.1016/j.bios.2021.113154

Wang C, Wang T, Li Z, Xu X, Zhang X, Li D. 2021. An electrochemical enzyme biosensor for ammonium detection in aquaculture using screen – printed electrode modified by gold nanoparticle / polymethylene blue. *Biosensors* 11 (9) : 335 ; https://doi.org/10.3390/bios11090335

Wang C, Yin J, Han S, Jiao T, Bai Z, Zhou J, Zhang L, Peng Q. 2019. Preparation of palladium nanoparticles decorated polyethyleneimine / polycaprolactone composite fibers constructed by electrospinning with highly efficient and recyclable catalytic properties. *Catalysts* 9 : 559 ; https://doi.org/10.3390/catal9060559

Zaak H, Fernandez – Lopez L, Otero C, Sassi M, Fernandez – Lafuente R. 2017. Improved stability of immobilized lipases via modification with polyethyleneimine and glutaraldehyde. *Enzyme and Microbial Technology* 106 : 67 – 74 ; http://dx.doi.org/10.1016/j.enzmictec.2017.07.001

Zdarta J, Staszak M, Jankowska K, Kazimierczak K, Degorska O, Nguyen LN, Kijenska – Gawronska E, Pinelo M, Jesionowski T. 2020. The response surface methodology for optimization of tyrosinase immobilization onto electrospin polycaprolactone – chitosan fibers for use in Bisphenol A removal. *Int J of Biological Macromolecules* 165 : 2049 – 2059 ; https://doi.org/10.1016/j.ijbiomac.2020.10.081

Zinchenko OA, Shkotova LV, Kulynych TU, Zinkina OO, Soldatkin AP. 2017. Highly selective amperometric biosensor for uric acid determination in real samples. *Biopolymers and Cell* 33 (2) : 124 – 134 ; http://dx.doi.org/10.7124/bc.00094A

CURICCULUM VITAE

Name Surname **:** Fakhriy MUHAMMAD

EDUCATION STATUS:

Bachelor **:** 2015, Bogor Agricultural University (IPB), Bogor, Indonesia, Faculty of Mathematics and Natural Sciences, Biochemistry

Master **:** 2022, Inonu University, Malatya, Turkey, Faculty of Sciences and Literature, Chemistry

WORKING EXPERIENCE **:**

Lab Assistant Department of Biochemistry IPB, Bogor, Indonesia (2014 – 2016)

Visiting Research Internship Protein Analytic Group Justus Liebig Univ (JLU) Giessen, Germany (Oct – Dec 2016)

Chemistry Teacher Laskar UI Education Center (2017 – 2018)

ACHIEVEMENTS **:**

Tubitak Research scholarship recipient 2020 – 2022

Karya Salemba Empat Bachelor Scholarship recipient 2013 – 2015

Hessen International Summer University Scholarship recipient, JLU Giessen, Germany July – August 2012

PUBLICATIONS **:**

1. Topsoy OK, Muhammad F, Kolak S, Ulu A, Gungor O, Simsek M, Koytepe S, Ates B. 2022. Fabrication of electrospin polycaprolactone/chitosan nanofiber – modified screen – printed electrode for highly sensitive detection of diazinon in food analysis. *Measurement* 187: 110250 ; https://doi.org/10.1016/j.measurement.2021.110250 .